Environmental Sciences Europe

RESEARCH

Open Access

Exploring a GIS-based analytic hierarchy process for spatial flood risk assessment in Egypt: a case study of the Damietta branch

Mohamed Zhran[1*], Karim Ghanem[1], Aqil Tariq[2], Fahad Alshehri[3], Shuanggen Jin[4,5], Jayanta Das[6], Chaitanya Baliram Pande[7,8], Malay Pramanik[9], Fahdah Falah Ben Hasher[10] and Ashraf Mousa[11]

Abstract

Floods are the most common and costly disasters worldwide, while spatial flood risk assessment is still challenging due to fewer observations and method limitations. In this study, the flood risk zonation in the Nile districts of the Damietta branch, Egypt, is delineated and assessed by integrating remote sensing with a geographic information system, and an analytical hierarchy process (AHP). Twelve thematic layers (elevation, slope, normalized difference vegetation index, topographic wetness index, modified normalized difference water index, topographic positioning index, stream power index, modified Fournier index, drainage density, distance to the river, sediment transport index, and lithology) are used for producing flood susceptibility zonation (FSZ) and six parameters (total population, distance to hospital, land use/land cover, population density, road density, and distance to road) are utilized for producing flood vulnerability zonation. Multicollinearity analysis is applied to identify highly correlated independent variables. Sensitivity studies have been used to assess the effectiveness of the AHP model. The results indicate that the high and very high flood risk classes cover 21.40% and 8.26% of the area, respectively. In 14.07%, 27.01%, and 29.26% of the research area, respectively, flood risk zones classified as very low, low, and moderate are found. Finally, FSZ is validated using the receiver operating characteristics curve and area under curve (AUC) analysis. A higher AUC value (0.741) in the validation findings demonstrated the validity of this AHP approach. The results of this study will help planners, hydrologists, and managers of water resources manage areas that are susceptible to flooding and reduce potential harm.

Keywords Flood risk assessment, AHP, Sensitivity analysis, Multiple criteria decision analysis (MCDA), Remote sensing and GIS, ROC, AUC

*Correspondence:
Mohamed Zhran
mohamedzhran@mans.edu.eg
[1] Public Works Engineering Department, Faculty of Engineering, Mansoura University, Mansoura 35516, Egypt
[2] Department of Wildlife, Fisheries and Aquaculture, College of Forest Resources, Mississippi State University, Mississippi State, MS 39762, USA
[3] Geology and Geophysics Department, College of Science, Abdullah Alrushaid Chair for Earth Science Remote Sensing Research, King Saud University, 11451 Riyadh, Saudi Arabia
[4] School of Surveying and Land Information Engineering, Henan Polytechnic University, Jiaozuo 454003, China
[5] Shanghai Astronomical Observatory, Chinese Academy of Sciences, Shanghai 200030, China
[6] Department of Geography, Rampurhat College, Birbhum, Rampurhat 731224, India
[7] New Era and Development in Civil Engineering Research Group, Scientific Research Center, Al-Ayen University, Thi-Qar, Nasiriyah 64001, Iraq
[8] Institute of Energy Infrastructure, Universiti Tenaga Nasional, 43000 Kajang, Malaysia
[9] Urban Innovation and Sustainability, Department of Development and Sustainability, Asian Institute of Technology (AIT), Pathum Thani 12120, Thailand
[10] Department of Geography and Environmental Sustainability, College of Humanities and Social Sciences, Princess Nourah Bint Abdulrahman University, P.O. BOX 84428, 11671 Riyadh, Saudi Arabia
[11] Geodynamic Department, National Research Institute of Astronomy and Geophysics, Helwan 11421, Egypt

Introduction

A natural disaster is a significant unfavorable occurrence brought on by Earth's natural processes. These can include earthquakes, tsunamis, volcanic eruptions, floods, storms, tornadoes, etc. [1]. Flooding is by far the most common natural hazard. In recent decades, it has significantly harmed the environment and caused socioeconomic harm in many regions of the world [2–4]. Floods are the most damaging natural catastrophes in the world, with the greatest number of fatalities and property destruction [1]. A flood is an excessive flow of water that submerges land, can destroy urban and agricultural regions, and sometimes even results in fatalities [5, 6]. To maintain long-term socioeconomic progress, geographers, hydrologists, hydrogeologists, and policymakers have found that assessing flood risk zonation (FRZ) has become an intriguing and creative issue in recent times [7]. The FRZ is dependent on the flood susceptibility zonation (FSZ) and flood vulnerability zonation (FVZ) of the relevant study region. Therefore, it is essential to model FSZ and FVZ to build the FRZ evaluation [8].

Multi-criteria decision analysis (MCDA), which was frequently utilized to simulate various types of FSZ, FVZ, and FRZ, is one of the most appropriate methods [7, 9]. Numerous techniques for mapping the susceptibility of natural hazards like floods have been developed, such as frequency ratio (FR) [10–12], Analytical Hierarchy Process (AHP) [3, 8, 10, 13, 14], Fuzzy Analytical Hierarchy Process (FAHP) [15], Vise Kriterijumska Optimizacijaik Ompromisno Resenje (VIKOR), Technique for Order Preference by Similarity to Ideal Solution (TOPSIS), and Evaluation Based on Distance from Average Solution (EDAS) [16].

Remote sensing (RS) and geographic information systems (GIS) have been effective over the past few decades in managing substantial hydrological information to produce more precise maps of flood susceptibility [17]. Furthermore, advancements in RS and GIS technology have facilitated the rapid identification of FRZ across large regions. Flood mapping using the AHP and GIS has gained popularity [10]. Furthermore, since its introduction by Saaty in 1971, the AHP has been widely applied as a helpful tool for multiple-criteria decision-making or a weight estimate approach in a variety of scenarios connected with human needs and interests [18]. The goal of AHP is to help decision-makers choose the option and set of criteria that best fit their objectives [19]. AHP is a convenient method for producing FRZ. This process results in a flood risk map that displays the spatial distribution of flood risk as well as the risk's intensity, which ranges from very high to very low.

Susceptibility is a characteristic that can be used to indicate a system's weakness or element exposed to a threat [20]. The term vulnerability describes the potential effects or damage, of an event occurrence [16]. In contrast to susceptibility, which is primarily focused on the physical environment, vulnerability is primarily defined by the socioeconomic restrictions of the hazardous occurrence, as few recent studies [21, 22] have clearly shown. The first step in anticipating and reducing the risk of future floods is to conduct a flood analysis. In this study, flood susceptibility and vulnerability are analyzed. Flood risk is determined by multiplying or adding the sum of the components of susceptibility and vulnerability. Many factors are generally responsible for FRZ, such as elevation, slope, drainage density, total population, population density, distance to river and so on [8].

Any model's cross-validation process has certain debatable research gaps, especially in the area of the criteria ratings that frame the model's outputs. The AHP method's sensitivity studies, which apply to any other study area, served as the foundation for the study's construction.

In the Nile Delta, ground levels are decreasing unevenly, with the northeastern region suffering a faster rate of subsidence than other areas [23]. Gebremichael et al. [23] reported that there are high subsidence rates (up to 8.9 mm/year) over the north central and northeastern Delta. Gebremichael et al. [23] reported that there are also high subsidence rates (up to 9.7 mm/year) in the southern delta (Menoufia governorate). Hence, these are the main causes leading to flooding in these areas. In addition to changes in land use (encroachments on watercourses) and inadequate flood protection management. Additionally, Coastal subsidence may exacerbate flooding caused by sea level rise. In general, the Damietta Nile branch meet the Mediterranean Sea at Ras El Bar. Hence, there is a relation between seal level rise and river flooding.

The Egyptian Meteorological Authority stated on March 11, 2020, that heavy rainfall and maybe flooding would occur between March 12 and 14, 2020. Government, public, and private sectors have been disrupted due to the government's request for residents to stay inside their houses and the closure of many important provincial routes. The total number of affected families in El-Qalyubia, El-Menofia, El-Gharbyia, El-Dakahlyia, and Damietta is 35, 149, 35, 10, and 3, respectively [24].

There was no study conducted in the study area and its surroundings by other researchers covering FSZ, FVZ, and FRZ using modern technology such as GIS and remote sensing in the study area. This study fills that gap and may be useful for flood risk mitigation. The main purposes of this paper are: (1) delineation of FSZ, FVZ,

and FRZ in the Nile districts of the Damietta branch of Egypt by integrating RS and GIS with the AHP after performing a multicollinearity test on the flood parameters; (2) evaluating the AHP's performance using sensitivity analysis, and (3) validating the model's accuracy using the receiver operating characteristic curve (ROC). In general, the results of this research will aid decision-makers, engineers, and local authorities in managing flood risks. Additionally, they will also aid in the creation of a strategic plan for urban growth and serve as a resource for future flood risk mitigation.

Study area

Damietta branch in Egypt, one of the two main branches of the River Nile, passes through five governments: El-Qalubia, El-Menofia, El-Gharbyia, El-Dakahlyia, and Damietta. With an average width of 200 m and an average depth of 12 m, Damietta branch extends about 242 km. The Nile districts of the Damietta branch are located between latitudes 30° 6' N to 31° 31' N and longitudes 30° 29' E and 32°5' E. The average annual precipitation in Damietta is about 9.18 mm [25]. The specific details of the research area in this study are illustrated in Fig. 1. The study area has approximately a population of 24 million

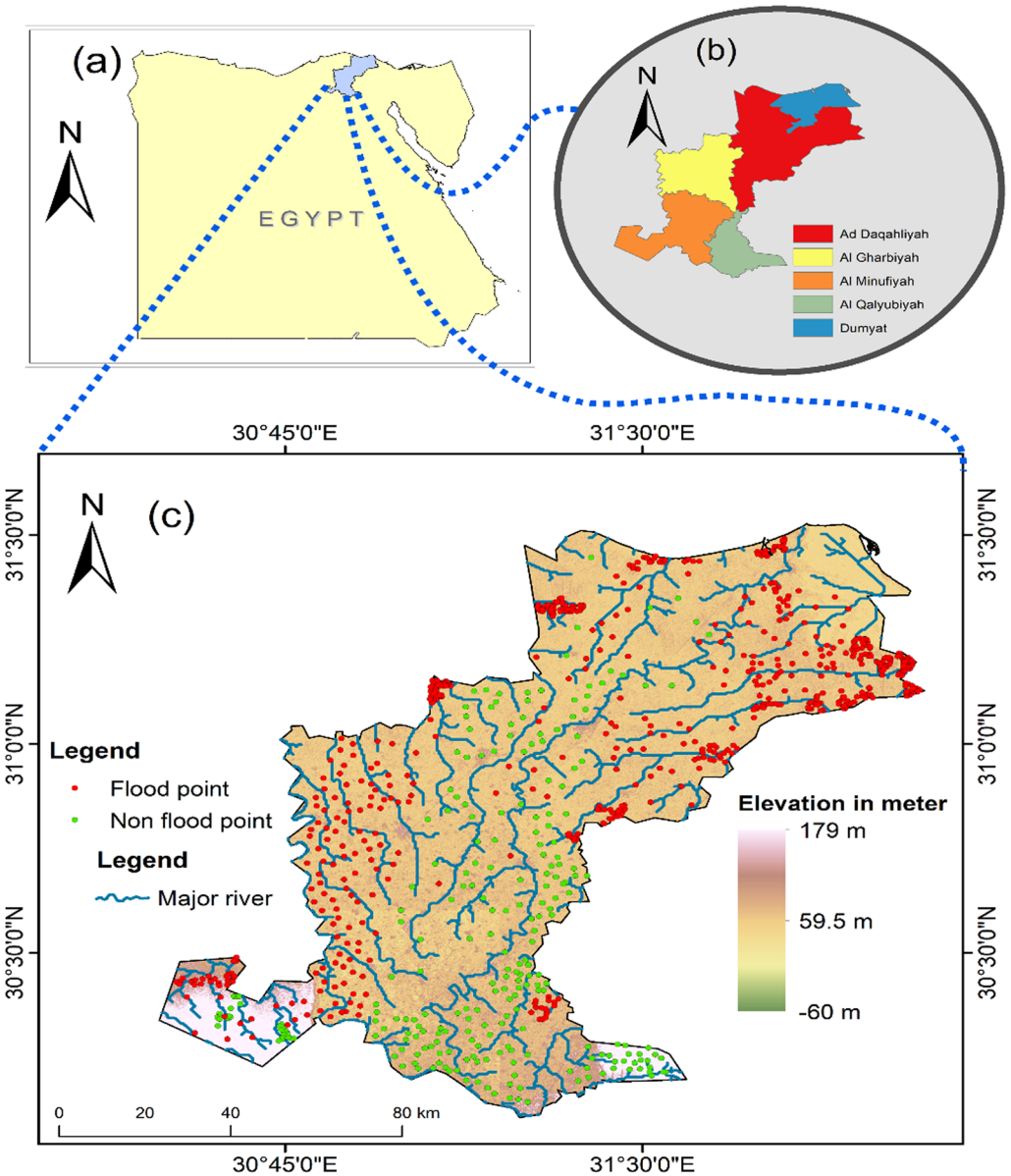

Fig. 1 Map of the study area: **a** Egypt map, **b** Nile districts of the Damietta branch, and **c** Damietta branch with flooded and non-flooded points

(Census 2021). The elevation ranges from − 60 to 179 m. The research area's slope varies from 0° to 46.75°, and about 59.15% of the study area was flat (0°–2°). Figure 1 combines the study area map with the flood inventory map. To prepare a flood inventory map, 658 flooded points and 265 non-flooded points have been chosen for additional investigation. The historical flood data are not available in this area, so we prepared the flood points using Synthetic Aperture Radar (SAR) data processing through Google Earth Engine platform. Changes in land use (Encroachments on watercourses) and ineffective flood prevention management are the major causes of flooding in these areas.

Methodology

Datasets

For the research region, 30-m resolution digital elevation model (DEM) data were acquired from the NASA Earthdata website (https://search.earthdata.nasa.gov; accessed on 15 June 2023). DEM was used to construct maps of the topographic factors such as elevation, slope, sediment transport index (STI), topographic positioning index (TPI), topographic wetness index (TWI), and stream power index (SPI). Additionally, the Landsat 8 satellite images obtained from the United States Geological Survey (USGS) are used to produce the NDVI and MNDWI. Landsat 8 satellite images are radiometrically corrected in the GIS platform and prepared for estimating the parameters NDVI, and MNDWI. Using Sentinel satellite images, LULC are produced. MFI is prepared using the gridded data (0.5 × 0.5) of the rainfall data from NASA Power. The OpenStreetMap website's data were used to construct the spatial layers for road density, distance to hospital, and distance to road. Total population and population density are estimated based on 2021 census obtained from central agency for public mobilization and statistics. Table 1 presents the source and description of the parameters used in the study. These data are used to determine Flood susceptibility parameters (FSP) and Flood vulnerability parameters (FVP). The principle of our method used in the study is illustrated in Fig. 2. FSP and FVP must be estimated to identify FRZ according to the methodology shown in Fig. 2.

Flood susceptibility parameters (FSP)

Twelve thematic layers are used for producing FSZ. Figures 3 and 4 present the distribution of the 12 FSPs used in this study.

Elevation

As water flows from higher to lower altitudes, it tends to accumulate [16]. Hence, elevations are a significant factor in identifying which locations are susceptible to floods [26]. Flooding has an inverse relationship with elevation [27]. The elevation map is estimated from the DEM [28].

Table 1 Source and description of the parameters used in the study

Parameter	Description	Source
Elevation, slope, TWI, TPI, SPI, STI, drainage density and distance to river	Derived from ASTER DEM (30m × 30m) and prepared the thematic layer using ArcGIS	United States Geological Survey (USGS) obtained from: https://earthexplorer.usgs.gov
NDVI and MNDWI	Using Landsat 8 (30m × 30m), all the layers were prepared after mosaicing and atmospheric correction of the image	USGS obtained from: https://earthexplorer.usgs.gov
LULC	Using Sentinel-2 (10m × 10m)	Copernicus Open Access Hub Retrieved from: https://scihub.copernicus.eu/
MFI	MFI Gridded rainfall (0.5 × 0.5) NetCDF	NASA Power LARC (0.5 × 0.5) https://power.larc.nasa.gov/
Lithology	Digital lithological map of the district	The Regional Centre for Mapping of Resources for Development (RCMRD) https://rcmrd.africageoportal.com/
Distribution of population, total population number Population density	Census of Egypt, 2021	Central Agency for Public Mobilization and Statistics
Distance to hospital, distance to road and road density	Adopting the data from OpenStreetMap	OpenStreetMap Retrieved from: www.openstreetmap.org

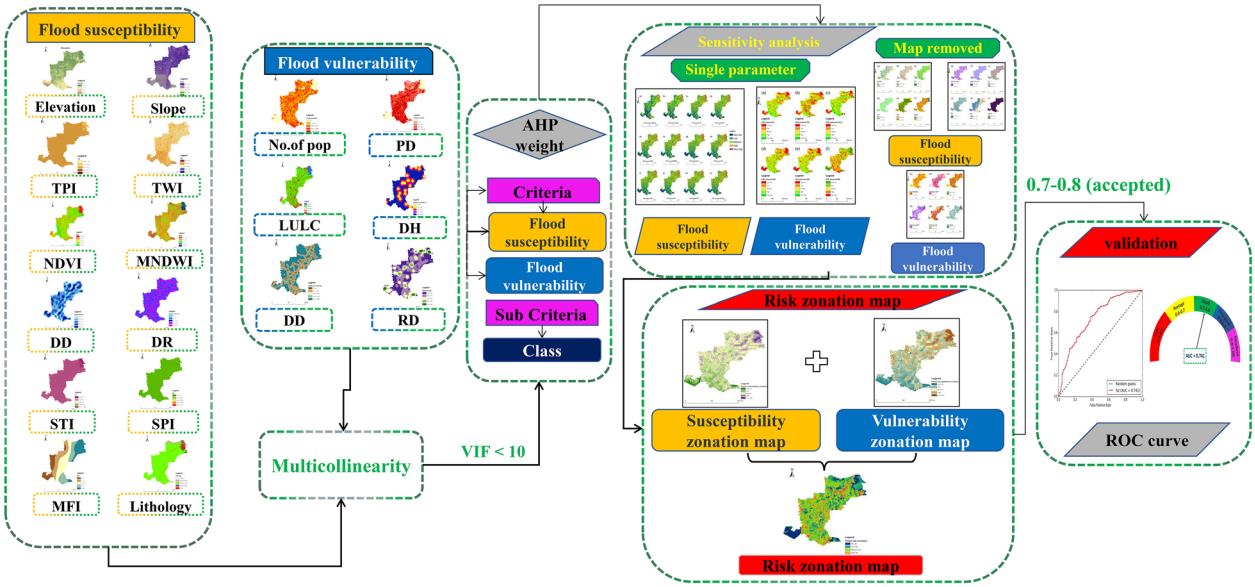

Fig. 2 The overall methodology adopted in this research

In the study area, the elevation varies from − 60 to 175 m, as shown in Fig. 3a.

Slope

The slope is another significant FSP since it directly influences the amount of surface runoff in any region [3, 27]. Steep slopes are less likely to cause flooding than flatter terrain; in other words, the risk decreases with increasing slope [29]. The slope map is produced from DEM. The slope of the target area varies from 0° to 46.75°, as illustrated in Fig. 3b.

Topographic wetness index (TWI)

Water movement overland is regulated by the TWI, which describes the geographical distribution of wetness [12]. The TWI, which is determined by combining the specific area of a basin and the slope angle of the region (in degrees) (B), is widely used to measure the topographic effect on hydrological processes [30]. DEM determines TWI. The region with a higher TWI rating indicates a higher probability of a flood occurrence [13]. Equation (1) was used to calculate the TWI, which is related to water flow [31]:

$$\mathrm{TWI} = \mathrm{Ln}\left(\frac{a}{\tan B}\right) \tag{1}$$

where a describes the upslope area (per unit contour length). Moreover, here $a = \frac{A}{L}$, where A is the total basin area, and L is the length of the contour [12, 31]. TWI distribution in the target area varied from 3.43 to 17.24, as presented in Fig. 3c.

Topographic positioning index (TPI)

TPI generally illustrates the altitudinal difference of each cell to the average altitude of surrounding cells in a specific radius [32]. The primary data for estimating TPI is DEM. TPI has a significant influence on runoff. For the investigations on flood susceptibility, TPI is chosen [8, 32]. The TPI is determined using Eqs. (2) and (3), where z_0 is the central point, $\bar{z}$ is the average elevation surrounding the central point, and R is the predetermined radius. TPI values ranged from − 4.66 to 4.41 in the target area, as presented in Fig. 3d:

$$TPI = z_0 - \bar{z} \tag{2}$$

$$\bar{z} = \frac{1}{n_R}\sum_{i \in R} Z_i \tag{3}$$

Normalized difference vegetation index (NDVI)

NDVI is considered a significant FSP [17, 33]. NDVI represents the normalized difference between the near-infrared band (NIR) and red light (Eq. (4)):

$$NDVI = \frac{NIR - RED}{NIR + RED} \tag{4}$$

The NDVI is used to identify regions covered in and not covered in vegetation. NDVI ranges from − 1 to 1. Regions with high vegetation cover less vulnerable to runoff from rainfall [29]. The spatial distribution of NDVI

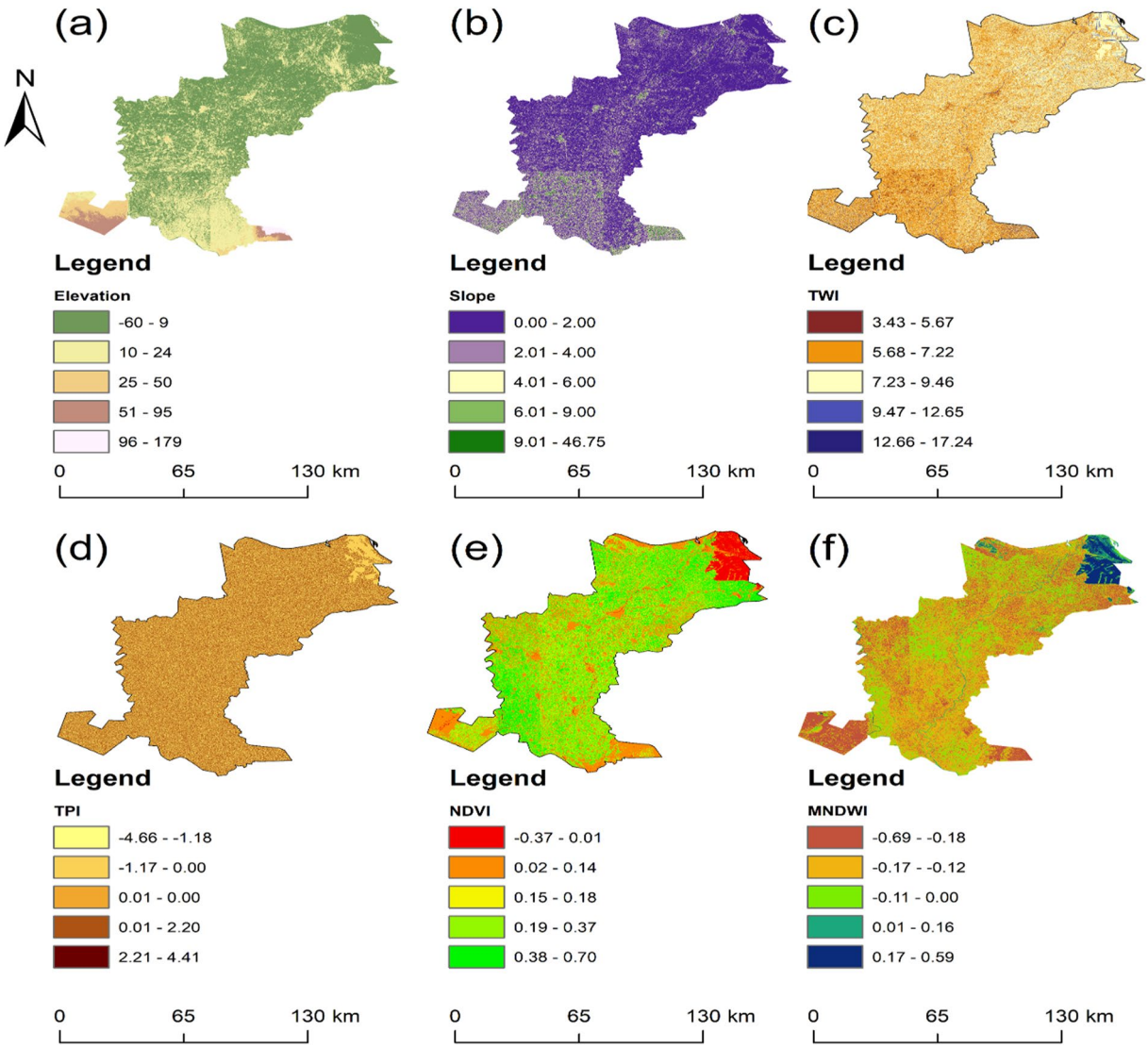

Fig. 3 Distribution of six FSPs used in this research: **a** elevation, **b** slope, **c** TWI, **d** TPI, **e** NDVI, and **f** MNDWI

varied from − 0.37 to 0.7 in the target area, as presented in Fig. 3e.

Modified normalized difference water index (MNDWI)

In this study, MNDWI is used as an FSP instead of the normalized difference water index (NDWI) as proposed by [8, 16]. In comparison to the NDWI, the MNDWI can effectively remove information about built-up regions and improve open water features when displaying them in locations with a higher concentration of built-up land. Consequently, Eq. (5) is used to estimate MNDWI [34]:

$$MNDWI = \frac{\text{Green} - MIR}{\text{Green} + MIR} \quad (5)$$

where MIR is as a middle infrared band. The MNDWI varies from − 0.69 to 0.59 in the target area, as shown in Fig. 3f.

Drainage density (DD)

Floods are mostly caused by the DD [7, 8]. The drainage network's length per unit area is represented by DD [10]. It has an impact on peak flow occurrences [32], runoff rates, and infiltration [16]. The DD is an important parameter for flood occurrence. The runoff rate is critical when the DD is high, causing an increase in flood volume [32]. DD (km/km^2) was estimated with the line density tool. DD can be computed from Eq. (6):

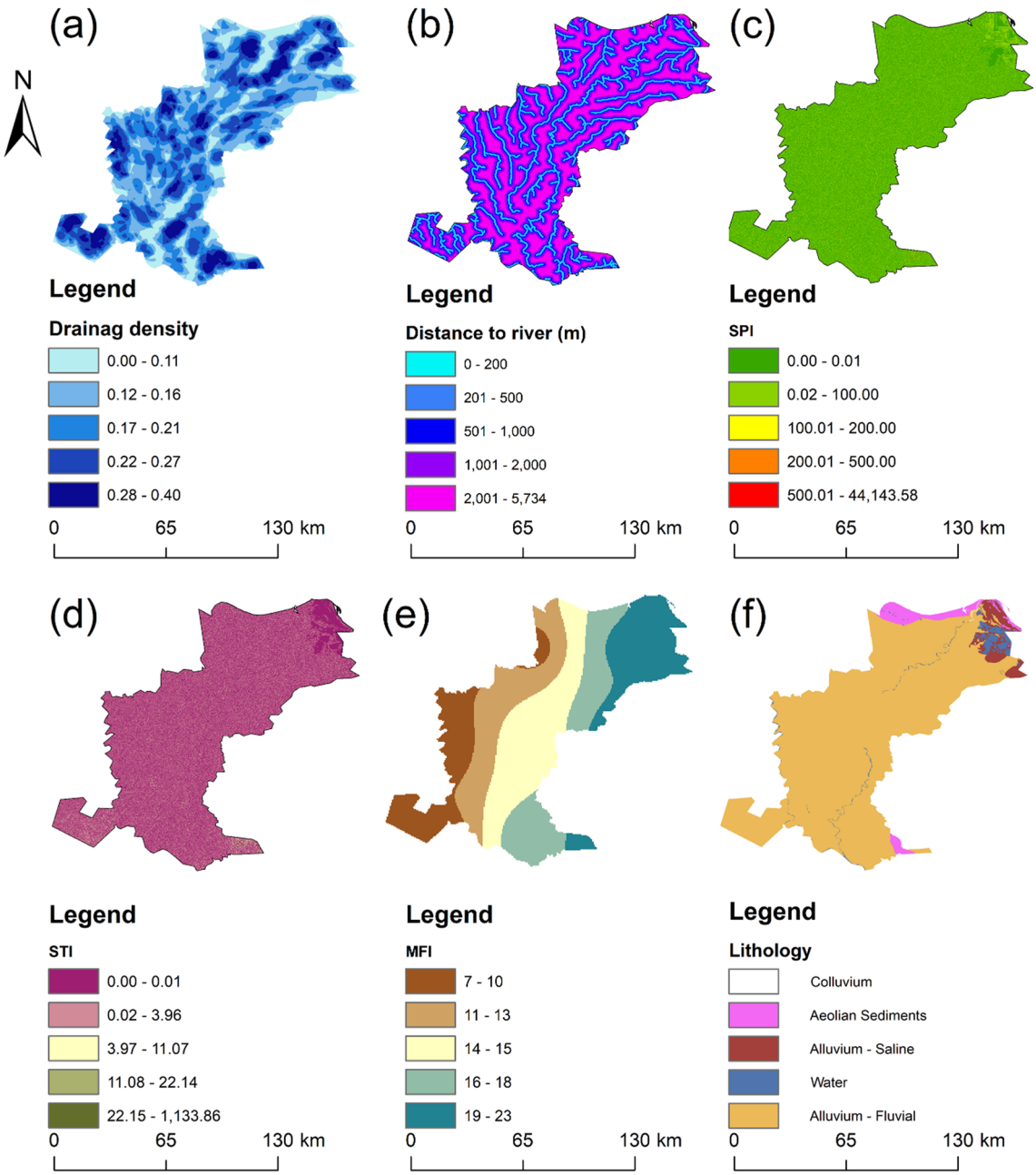

Fig. 4 Distribution of another six FSPs used in this research: **a** DD, **b** DR, **c** SPI, **d** STI, **e** MFI, and **f** lithology

$$DD = \frac{L}{A} \tag{6}$$

where L describes the total length of the drainage channel in the watershed (km) and A describes the total area of the watershed (km^2). The DD map in the target area ranged from 0 to 0.4 km/km^2, as revealed in Fig. 4a.

Distance to the river (DR)

One major parameter influencing the likelihood of flooding is the DR [3, 27, 35]. In locations close to the main river channel and flow accumulation path, flooding is more likely to occur [10, 27, 36]. On the other hand, areas further from rivers are less susceptible to flood damage. The DR is estimated in ArcGIS Pro 2.8.4 using the Euclidean distance method. The DR in the target area ranged from 0 to 5734 m, as described in Fig. 4b.

Stream power index (SPI)

The SPI displays the stream flow's erosive power [37]. It is the product of the catchment area (Ai) and slope (β) and estimates the force of the water flows at a specific watershed. Greater SPI values indicate increased potential for flooding in the region's rivers [16]. The SPI is computed using Eq. (7) [38]:

$$SPI = Ai * \tan\beta \tag{7}$$

The equation mentioned above was used to produce the SPI map from the DEM. The spatial distribution of SPI in the target area varied from 0 to 44,143.58, as presented in Fig. 4c.

Sediment transport index (STI)

Another important flood susceptibility metric is the STI. It is connected to any region's runoff features. Lower STIs are connected to areas that are more susceptible to flood and vice versa [39]. The STI is computed through Eq. (8), where F_a is the flow accumulation and S_α is the slope raster, obtained from DEM, and δx and δy stand for the constant [8, 16, 39]. The STI map in the target area ranged from 0 to 1133.86, as described in Fig. 4d:

$$STI = \left[\frac{\left(\frac{F_a}{\delta x}\right)^{\wedge 2}}{\left(\frac{\text{sign}(S_\alpha)}{\delta y}\right)^{\wedge 2}} \right] \tag{8}$$

Modified Fournier index (MFI)

The MFI is used to represent rainfall intensity. The most frequent cause of floods is intense rainfall. Given that higher MFI values are associated with areas that are very susceptible to flooding, it was regarded as a crucial flood conditioning variable [7]. MFI is obtained by Eq. (9) [7, 40]:

$$MFI = \sum_{i=1}^{12} \frac{P_i^2}{P} \tag{9}$$

where P_i describes the monthly average of precipitation for month i (mm), and P describes the average annual precipitation (mm). The MFI in the target area ranged from 7 to 23 mm/year, as described in Fig. 4e.

Lithology

Lithology is one of the significant factors in the determination of the FSZ [7]. It impacts the properties of the drainage network in any area, as well as soil permeability and hydrological processes. There is less drainage density in areas with extremely permeable subsoil or very resistant rocks [35, 41]. Consequently, it is assumed that a crucial flood conditioning parameter is the local lithological structure [8]. The lithological map of the study area is presented in Fig. 4f.

Flood vulnerability parameters (FVP)

Six parameters are used for producing FVZ. Vulnerability is controlled and influenced by physical/natural factors. Figure 5 introduces the distribution of the six FVPs used in this study.

Total population (TP)

One key metric used to evaluate flood vulnerability is population [8]. The growing population causes an acceleration of environmental vulnerability. The population census in this study was conducted in 2021. The total population of the target area is approximately 24 million (2021 census), as observed in Fig. 5a.

Population density (PD)

PD is a crucial factor in assessing social vulnerability since floods may have a negative impact on people's physical and psychological health [14]. The ratio of residents to land area is known as population density, and it serves as an indicator of the economic growth of metropolitan areas [29]. High population density areas are particularly susceptible to flooding threats. The population density of the target area is depicted in Fig. 5b.

Land use land cover (LULC)

LULC is another crucial influencing factor that contributes to flood risk [7, 10, 42]. LULC affects surface runoff, rate of evapotranspiration, evaporation, and infiltration [7, 37]. A vegetated region minimizes the amount of surface runoff. It increases the progress of the infiltration process. In contrast, a built-up area severely hinders the infiltration of water into the ground and speeds up the surface flow [9]. Based on Sentinel satellite images, these LULC classifications are established. Most of the area is classified as vegetation covers as shown in Fig. 5c.

Distance to hospital (DH)

A key factor in determining an area's vulnerability is how easily accessible medical facilities are, as well as how close they are to people's homes [8]. The impacts of a disaster can be significantly reduced if every affected person has instant access to the hospital [14]. The distance to the hospital is obtained from the open street map data website. The distance to the hospital map of the target area is introduced in Fig. 5d.

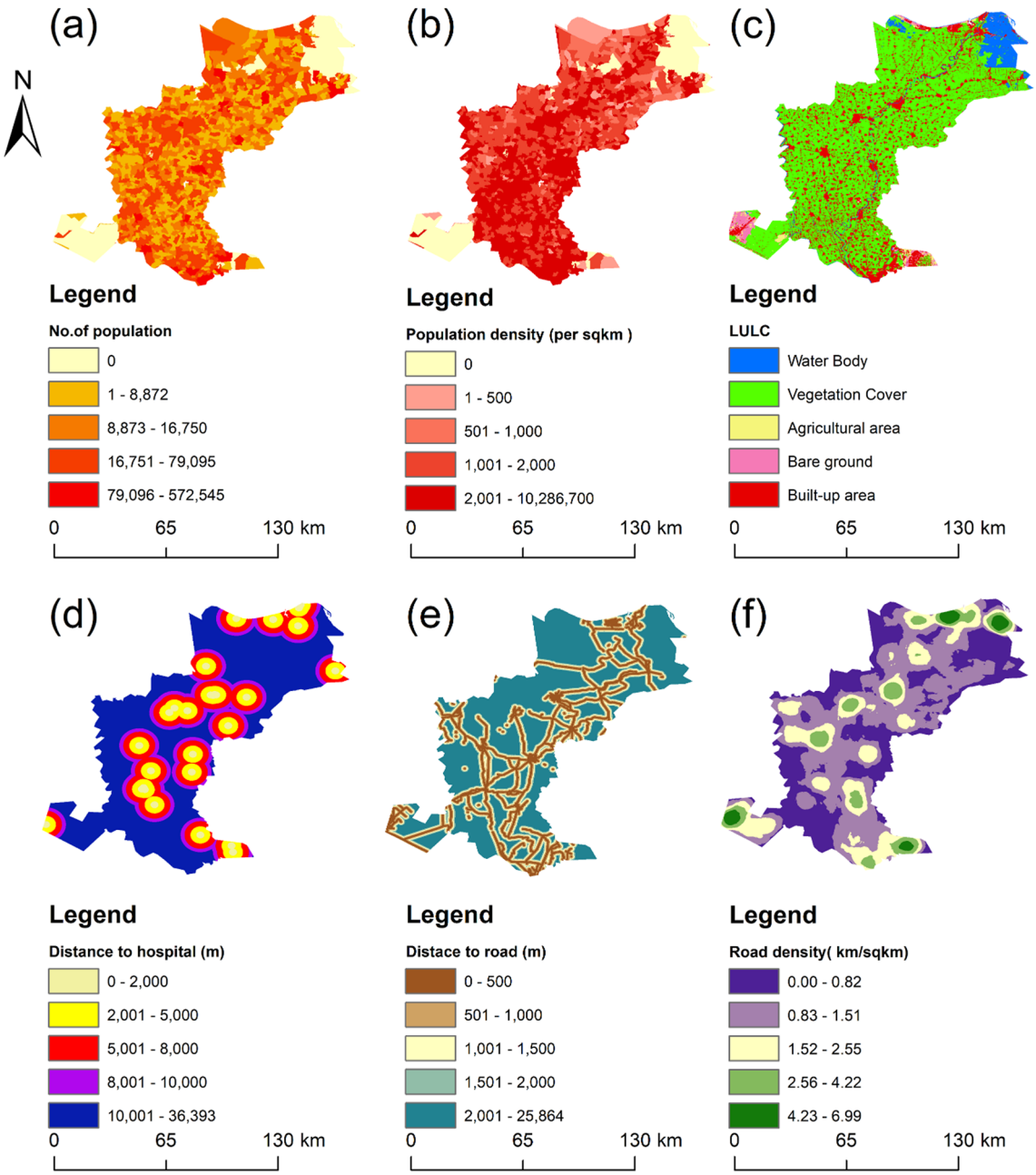

Fig. 5 Distribution of six FVPs used in this research: **a** TP, **b** PD, **c** LULC, **d** DH, **e** DTR, and **f** RD.

Distance to road (DTR)

A further essential factor in estimating FVZ is the DTR. Because roads act as manufactured barriers to floodwaters, they prevent flooding [11]. The distance to the road is obtained from the open street map data website. The DTR of the study area is presented in Fig. 5e.

Road density (RD)

The density of the road network is the proportion of road km to the regional area, which is a measure of urbanization [29]. High road density considerably slows down the progress of flood damage [11]. The road density is obtained from the open street map data website. In Fig. 5f, we can observe the road density map in the study area.

Multicollinearity checks

Multicollinearity (MC) is the phenomenon of correlation among two or more independent variables [43]. The current study analyses the use of MC analysis to identify significantly related independent variables. MC analysis is a crucial tool for evaluating the efficacy of susceptibility and vulnerability parameters.

In this study, MC was measured by the variance inflation factor (VIF) and tolerance (T) for each susceptibility and vulnerability parameter. A tolerance of less than 0.10 and a VIF of 10 or above indicates MC problems [44]. ArcGIS 10.5 was also utilized to create and extract the random points in each theme layer for the MC study. The MC test was run using SPSS software.

Equations (10) and (11) were used to determine the VIF for any predictor variable (Myers and Well, 2003):

$$\text{VIF of the } i^{th} \text{ variable } (\text{VIF}_\text{i}) = \frac{1}{\text{T}_\text{i}} \tag{10}$$

$$\text{Tolerance of the } i^{th} \text{ variable } (\text{T}_\text{i}) = 1 - \text{R}_\text{i}^2 \tag{11}$$

R_i^2 is the determination coefficient of the equation of regression.

Weighting and ranking of each layer by AHP

Saaty initially presented the AHP multicriteria decision approach in 1980, and it is now a helpful and common technique [18]. The AHP approach is applied to evaluate the weight of several layers. In this study, 12 FSPs were used to generate the FSZ, and six FVPs were applied to create the FVZ. We developed a pairwise comparison matrix (PCM) based on FSP and FVP, which was considered the initial step. Determining the normalized weights is the second step in this approach. Hence, each thematic layer was given a relative weight based on Saaty's scale of 1 to 9. Each layer's relative weight has been established using a literature review, field experience, research in similar geographic areas, and the study by Mitra et al. [8]. PCM is used to compute parameter weight, class weight, and the consistency ratio (CR) value.

Consistency analysis

By calculating the CR using Eq. (12), the judgments made about the PCM of thematic layers and subclasses within those layers were validated [45]:

$$CR = \frac{CI}{RI} \tag{12}$$

As listed in Table 2, the values of the random index (RI) used to compute consistency were taken from Saaty's standard, and the consistency index (CI) values were computed using Eq. (13):

$$CI = \frac{(\lambda_{max} - n)}{n - 1} \tag{13}$$

where λ_{max} is the maximum eigenvalue of the judgment matrix, and n is the number of criteria. In this study, the RI value is 1.48 for FSP since 12 parameters were provided and 1.24 for FVP since six parameters were used. A CR < 0.1 demonstrates an appropriate decision to continue the AHP analysis, according to [45].

Overlay analysis

The preparation of FSZ and FVZ is the important aim of this study. Equations (14) and (15) were used for the preparation of FSZ and FVZ as follows:

$$FSZ = \sum_{i=1}^{n} W_i^S \times R_i^S \tag{14}$$

$$FVZ = \sum_{i=1}^{n} W_i^V \times R_i^V \tag{15}$$

where W_i^S and W_i^V are the weights of FSP and FVP, respectively. R_i^S and R_i^V are the ranks of the subclasses of each thematic layer of FSP and FVP, respectively.

The main task of this study is modeling FRZ depending on FSZ and FVZ, as presented in Eq. (16):

$$FRZ = FSZ \times FVZ \tag{16}$$

Sensitivity analysis

To validate the allocated weight of AHP, the consequences of the sensitivity analysis are needed [43]. Single parameter sensitivity analysis (SPSA), map removal sensitivity analysis (MRSA), and Stillwell ranking technique (SRT) are employed in this study.

Single parameter sensitivity analysis (SPSA)

The reason for this sensitivity test is that the flood parameters have arbitrary integer values assigned to them

Table 2 Saaty's random index [45]

n	1	2	3	4	5	6	7	8	9	10	11	12	13	14	15
RI	0	0	0.58	0.90	1.12	1.24	1.32	1.41	1.45	1.49	1.51	1.48	1.56	1.57	1.59

n number of criteria, *RI* random index

[46]. The SPSA compares the weighting factor for each layer with the empirical weighting (EW) factor to determine the efficacy of each layer on the FSZ and FVZ maps [43, 47]. In this study, the effective weight (W) for FSZ and FVZ maps was determined using Eqs. (17) and (18):

$$W = \frac{P_r P_w}{\mathrm{FSZ}} \times 100 \tag{17}$$

$$W = \frac{P_r P_w}{\mathrm{FVZ}} \times 100 \tag{18}$$

where W is the effective weight, P_r and P_w are the rate and weight values of every layer, respectively.

Map removal sensitivity analysis (MRSA)

MRSA is used to determine the effects of removing any of the layers used for the determination of FSZ and FVZ maps. Each time a layer is removed, a new FSZ and FVZ maps arise from overlaying the remaining layers, and a sensitivity index (SI) related to an omitted layer is estimated using Eqs. (19) and (20) [43, 48]:

$$\mathrm{SI} = \frac{\left|\left(\frac{\mathrm{FSZ}}{\mathrm{N}}\right) - \left(\frac{\mathrm{FSZ'}}{\mathrm{n}}\right)\right|}{\mathrm{FSZ}} \times 100 \tag{19}$$

$$\mathrm{SI} = \frac{\left|\left(\frac{\mathrm{FVZ}}{\mathrm{N}}\right) - \left(\frac{\mathrm{FVZ'}}{\mathrm{n}}\right)\right|}{\mathrm{FVZ}} \times 100 \tag{20}$$

where FSZ and FVZ relate to all layers, and FSZ′ and FVZ′ denotes the FSZ and FVZ obtained by excluding one layer. N is the number of FSZ and FVZ layers maps, and n is the number of FSZ′ and FVZ′ layers maps.

Stillwell ranking technique (SRT)

SRT involves two weights, namely, rank sum weight ($W_i(RS)$) and reciprocal rank weight ($W_i(RR)$), which are utilized to compare with the AHP approach. The $W_i(RS)$ and $W_i(RR)$ are calculated using Eqs. 21 and 22, as proposed by Stillwell in 1981 [49]:

For rank sum weight:

$$W_i(RS) = (n - R_j + 1) / \sum_{k=1}^{n} (n - R_k + 1) \tag{21}$$

For reciprocal rank weight:

$$W_i(RR) = \frac{\frac{1}{R_j}}{\sum_{k=1}^{n} \left(\frac{1}{R_k}\right)} \tag{22}$$

Here, W_i represents each parameter's normalized weight, n is the number of parameters. The parameters are ranked in ascending sequence, R_j is each parameter's direct rank, and each weight is normalized by the sum of $\sum_{k=1}^{n} (n - R_k + 1)$ for all parameters.

Table 3 MC statistics of FSP and FVP

Susceptibility parameters	VIF	Vulnerability parameters	VIF
Elevation	1.535	No. of population	1.124
Slope	2.044	Population density	1.061
TWI	2.169	LULC	1.124
TPI	1.256	Distance to hospital	1.118
NDVI	1.354	Distance to road	1.095
MNDWI	1.898	Road density	1.135
DD	1.157		
DR	1.163		
SPI	1.054		
STI	1.012		
MFI	3.854		
Lithology	1.565		

Table 4 The consistency check results of FSP

n	RI	λ_{max}	CI	CR	Consistency
12	1.48	13.26	0.11	0.08	CR < 0.1 (yes)

n number of criteria, *RI* random index, λ_{max}, the maximum eigenvalue, *CI* consistency index, *CR* consistency ratio

Accuracy assessment

For validation purposes, the ROC is utilized [8, 13, 50]. The false-positive rate, which expresses the number of samples in the flood risk map where floods have not happened, is shown along the x-axis of an ROC curve graph. The number of samples in the flood risk map where floods have occurred is expressed by the true positive rate, which is shown along the y-axis. An indicator of the model's quality is the area under the curve (AUC) [8, 51]. The AUC has a range of 0 to 1. A higher AUC value indicates the model's superior quality.

Results and discussion

Multicollinearity analysis

In this study, 5000 random points were used for both FSP and FVP during the MC analysis. MC analysis results are listed in Table 3. From the analysis, it was found that STI (0.988) has the highest tolerance value, followed by SPI (0.949), whereas MFI (0.259) has the lowest tolerance value. The VIF values range from 1.012 (STI) to 3.854 (MFI). The results show that the VIF is less than 10, and the tolerance value exceeds 0.1 for all FSP and FVP. The results listed in Table 3 clearly show that there is no

Table 5 Weightage of each factor and sub-factor of FSP

Parameters	AHP weight	Reclass class	Class range	Flood level	Area (km^2)	Area (%)	Rating
Elevation	0.267	1	– 59–9	Very high	5921.32	59.48	0.416
		2	10–24	High	3352.17	33.67	0.262
		3	25–50	Medium	373.45	3.75	0.161
		4	51–95	Low	265.53	2.67	0.099
		5	96–179	Very low	42.73	0.43	0.062
Slope	0.192	1	0–2	Very high	5875.96	59.15	0.444
		2	2–5	High	3269.31	32.91	0.262
		3	5–7	Medium	481.34	4.85	0.153
		4	7–9	Low	182.59	1.84	0.089
		5	9–46.75	Very low	124.55	1.25	0.053
TWI	0.087	1	3.43–5.67	Very low	290.28	2.92	0.053
		2	5.68–7.22	Low	4500.91	45.21	0.089
		3	7.23–9.46	Medium	4650.74	46.72	0.153
		4	9.47–12.65	High	505.91	5.08	0.262
		5	12.66–17.24	Very high	7.35	0.07	0.444
TPI	0.015	1	– 4.66–-1.18	Very high	1191.03	11.91	0.489
		2	– 1.17–0	High	3997.49	39.97	0.261
		3	0	Medium	4.86	0.05	0.138
		4	0.01–2.20	Low	4704.63	47.04	0.073
		5	2.21–4.41	Very low	103.64	1.04	0.038
NDVI	0.028	1	– 0.37–0.01	Very high	478.65	4.81	0.416
		2	0.02–0.14	High	2664.62	26.77	0.262
		3	0.15–0.18	Medium	1240.15	12.46	0.161
		4	0.19–0.37	Low	3332.84	33.48	0.099
		5	0.38–0.70	Very low	2238.57	22.49	0.062
MNDWI	0.063	1	– 0.69–0.18	Very low	2721.65	27.34	0.056
		2	– 0.17–0.12	Low	4508.37	45.29	0.096
		3	– 0.11–0	Medium	2095.22	21.05	0.157
		4	0.01–0.16	High	136.92	1.38	0.257
		5	0.17–0.59	Very high	492.67	4.95	0.434
Drainage density (km/km^2)	0.123	1	0.00–0.11	Very low	1443.77	15.00	0.050
		2	0.12–0.16	Low	2900.58	29.00	0.088
		3	0.17–0.21	Medium	2729.66	27.00	0.151
		4	0.22–0.27	High	2009.78	20.00	0.259
		5	0.28–0.40	Very high	871.13	9.00	0.451
Distance from river	0.122	1	0–200	Very high	784.47	7.88	0.503
		2	201–500	High	1132.82	11.38	0.260
		3	501–1000	Medium	1807.01	18.15	0.134
		4	1001–2000	Low	3199.37	32.14	0.068
		5	2001–5734	Very low	3031.23	30.45	0.035
SPI	0.015	1	0–25,000	Very high	5484.12	55.09	0.503
		2	25,001–243,200	High	4447.94	44.68	0.260
		3	243,201–885,678	Medium	12.97	0.13	0.134
		4	885,679–3,206,497	Low	5.72	0.06	0.068
		5	3,206,498–7,235,901	Very low	4.45	0.04	0.035

Table 5 (continued)

Parameters	AHP weight	Reclass class	Class range	Flood level	Area (km^2)	Area (%)	Rating
STI	0.015	1	0.00–0.01	Very high	5721.93	57.48	0.503
		2	0.02–3.96	High	4084.55	41.03	0.260
		3	3.97–11.07	Medium	124.81	1.25	0.134
		4	11.08–22.14	Low	16.95	0.17	0.068
		5	22.15–1,133.86	Very low	6.96	0.07	0.035
MFI	0.044	1	7–10	Very low	1321.29	13.29	0.053
		2	11–13	Low	2520.77	25.35	0.089
		3	14–15	Medium	2224.21	22.37	0.153
		4	16–18	High	2260.28	22.73	0.262
		5	19–23	Very high	1615.72	16.25	0.444
Lithology	0.028	1	Colluvium	Very high	82.26	0.83	0.505
		2	Aeolian sediments	High	390.81	3.93	0.262
		3	Alluvium–saline	Medium	329.40	3.31	0.128
		4	Water	Low	234.49	2.36	0.069
		5	Alluvium–fluvial	Very low	8903.13	89.57	0.036

MC problem among the different parameters for both susceptibility and vulnerability.

Flood susceptibility zones

To prepare the FSZ, each thematic layer from the 12 FSP is classified into five categories. Tables SM1 and SM2 in the supplementary material (SM) list the PCM for FSP by AHP and the normalized weight for FSP for this study, respectively. The consistency check results of the FSP are summarized in Table 4. Table 5 lists the weightage of each factor and sub-factor of FSP.

The area with low elevations ranging from − 59 m to 9 m represents 59.48% of the target area and represents a very high flooding impact, as described in Table 5, as water moves from higher to lower. As a result, areas with very low elevations are more susceptible to floods. The area with high elevations varying from 96 to 179 m, which represents 0.43% of the study area, was classified as having a very low flooding impact. The elevation assigned about 27% of the AHP weight as the highest weight in all flood susceptibility parameters.

The slope is assigned about 19% of the AHP weight. About 59.15% of the study area was flat (0°–2°), and this represents a very high flooding impact, as reported in Table 5. As a result, locations with the lowest slopes get the most floods. Areas with a higher TWI are more susceptible to floods than other subclasses. Subsequently, the rating for higher values of TWI is higher than for lower values, as mentioned in Table 5. Zero TPI areas are flat, and negative TPI areas are areas with low elevations; hence, areas with zero or negative TPI are more susceptible to flooding. Hence, the rating for lower values of TPI is higher than for lower values (Table 5).

Areas with negative NDVI values indicate a high probability of flooding. Consequently, higher ratings were allocated for lower values of NDVI (Table 5) because an increase in vegetation cover decreased the probability of flooding. Higher values of MNDWI indicated water regions. Accordingly, higher ratings were allocated for higher values of MNDWI (Table 5) due to an increase in water area, increasing the probability of flooding.

The DD assigned about 12% of the AHP weight as the third highest weight in all flood susceptibility parameters after elevation and slope. The rating for higher values of DD is higher than for lower values (Table 5). The DR assigned about 12% of the AHP weight to the DD. Higher ratings were allocated for lower values of DR (Table 5) due to areas near the river being more susceptible to floods. The stronger the flow, the higher the SPI value. Areas with lower SPI values are more susceptible to flooding than other subclasses. Subsequently, the rating for lower SPI values is higher than for lower values, as mentioned in Table 4, due to lower SPI being linked to slow water flow.

The rating for lower values of STI is higher than for lower values (Table 5). Thus, the lower STI is more susceptible to flooding. Higher ratings were allocated for higher

Table 6 The consistency check results of FVP

n	RI	λ_{max}	CI	CR	Consistency
6	1.24	6.10	0.02	0.02	CR < 0.1 (yes)

Table 7 Weightage of each factor and sub-factor of FVP

Parameters	AHP Weight	Class	Range	Flood level	Area (km^2)	Area in %	Rating
Total population	0.292	1	0	Very low	1298.53	13.06	0.047
		2	0–2000	Low	2624.89	26.40	0.085
		3	2001–4000	Moderate	2611.59	26.27	0.150
		4	4001–10,000	High	3031.39	30.49	0.259
		5	10,001–572,545	Very high	374.53	3.77	0.459
Population density	0.292	1	0	Very low	1298.53	13.06	0.047
		2	1–500	Low	582.65	5.86	0.085
		3	501–1000	Moderate	1135.65	11.42	0.150
		4	1001–2000	High	3130.31	31.49	0.259
		5	2001–10,286,700	Very high	3793.80	38.16	0.459
LULC	0.176	1	Water body	Very low	625.03	6.28	0.035
		2	Vegetation cover	Moderate	7094.54	71.27	0.134
		3	Agricultural area	High	103.97	1.04	0.260
		4	Bare ground	low	191.85	1.93	0.068
		5	Built-up area	Very high	1939.45	19.48	0.503
Distance to hospital (m)	0.107	1	0–2000	Very low	295.48	2.97	0.049
		2	2001–5000	Low	1254.34	12.60	0.082
		3	5001–8000	Moderate	1818.47	18.27	0.149
		4	8001–10,000	High	1249.18	12.55	0.267
		5	10,001–36,393	Very high	5337.36	53.62	0.454
Distance to road (m)	0.075	1	0–500	Very low	1566.34	15.73	0.056
		2	501–1000	Low	1255.45	12.61	0.096
		3	1001–1500	Moderate	1055.98	10.61	0.157
		4	1501–2000	High	894.25	8.98	0.257
		5	2001–7699	Very high	5182.82	52.06	0.434
Road density	0.059	1	0.00–0.82	Very High	3246.26	32.61	0.426
		2	0.83–1.51	High	4177.69	41.97	0.259
		3	1.52–2.55	Medium	1715.29	17.23	0.159
		4	2.56–4.22	Low	603.84	6.07	0.097
		5	4.23–6.99	Very low	211.83	2.13	0.059

values of MFI (Table 5). As a result, higher MFI means high susceptibility to flood. One of the key elements in the determination of the FSZ is lithology. It is categorized into five categories based on water holding capacity. The very high flood hazard (FH) class is connected to colluvium. In contrast, the high FH class is associated with aeolian sediments, the medium FH class is alluvium–saline, and the low FH class is with water. Very low F.H. classes are with alluvium–fluvial.

Flood vulnerability zones

To prepare the FVZ, each thematic layer from the six vulnerability parameters is classified into five categories. Tables SM3 and SM4 in the SM list the PCM for FVP by AHP and the normalized weight for FVP for this study, respectively. The consistency check results of the FVP are summarized in Table 6. Table 7 lists the weightage of each factor and sub-factor of FVP.

Population is related to flood vulnerability. The rating for higher values of population is higher than for lower values, as reported in Table 7. The total population is assigned about 29% of the AHP weight as the highest weight in all flood vulnerability parameters. Population density is related to flood vulnerability since more people are exposed to risk in densely populated areas. Subsequently, the rating for higher values of population density is higher than for lower values, as mentioned in Table 7. The population density is also assigned about 29% of the AHP weight as the highest weight in all flood vulnerability parameters.

In the investigation of flood vulnerability, the LULC is crucial. The LULC of the study area is presented in five classes, i.e., water body (6.28%), vegetation (71.27%), agricultural area (1.04%), bare ground (1.93%), and built-up area (19.48%). Built-up areas are classified as high-risk for flooding vulnerability, as listed in Table 7.

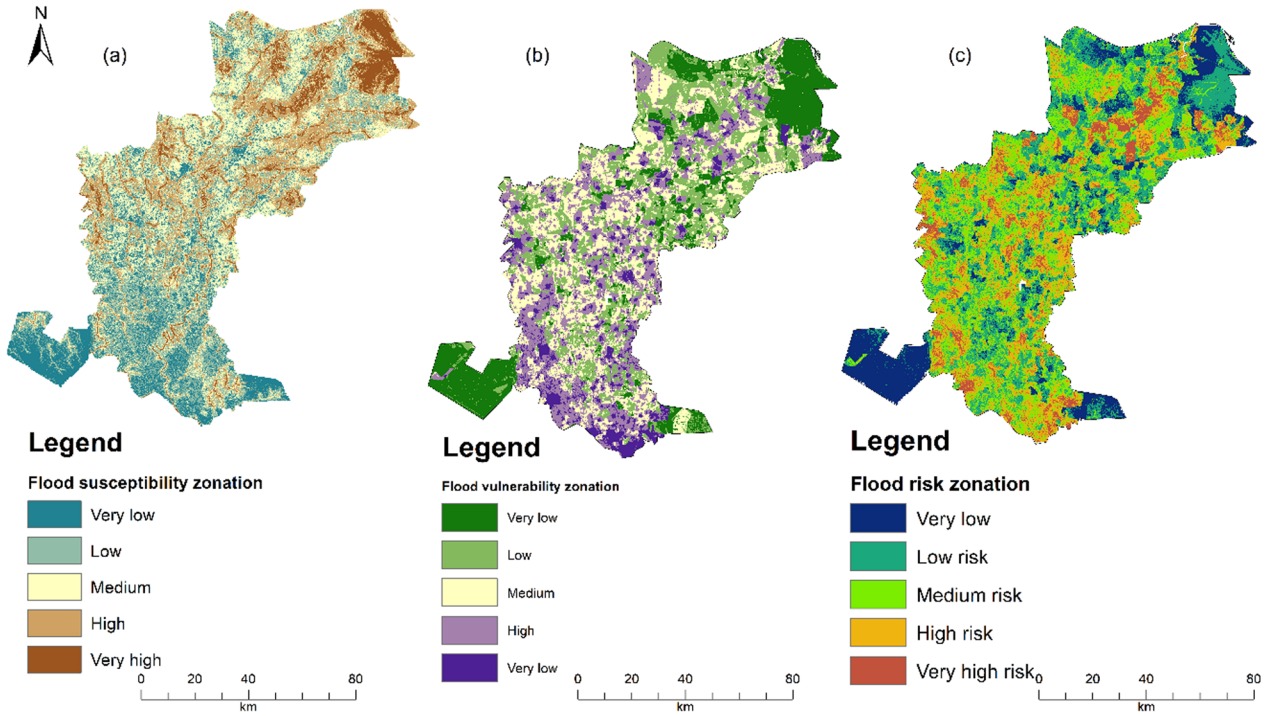

Fig. 6 **a** FSZ, **b** FVZ and **c** FRZ maps of the target area

Table 8 Area of FSZ, FVZ, and FRZ of the study area

Level	FSZ		FVZ		FRZ	
	Area (km^2)	Area (%)	Area (km^2)	Area (%)	Area (km^2)	Area (%)
Very low	1619.77	16.44	1851.62	18.64	1384.42	14.07
Low	2530.17	25.69	2361.14	23.77	2658.68	27.01
Medium	2823.32	28.66	2689.95	27.08	2880.07	29.26
High	2093.74	21.26	2307.62	23.23	2106.18	21.40
Very high	783.00	7.95	724.63	7.29	813.21	8.26

The maximum rating is assigned to the longest distance to the hospital, as given in Table 7. The higher rating is assigned to the longest distance to the road, as exhibited in Table 7. RD varies from very low at 0–0.82 to very high at 4.23–6.99 as listed in Table 7.

AHP model output

FSZ

The weighted overlay method is applied to produce FSZ from the 12 reclassified layers of FSP, as highlighted in Fig. 6a. FSZ map is categorized into five categories: very low, low, medium, high, and very high. The area of FSZ for each class is listed in Table 8.

FVZ

The weighted overlay method is applied to produce FVZ from the six reclassified layers of FVP, as presented in Fig. 6b. Five categories are used for categorizing the FVZ map: very low, low, medium, high, and very high. The FVZ area for each class is given in Table 8.

FRZ

The production of FRZ maps utilizing FSZ and FVZ maps is the main result of this study. The FRZ map is categorized into five classes: very low, low, medium, high, and very high. The FRZ area for each class is given in Table 8**.** Groups with very high and high flood risk covered 82.6% and 21.40% of the research region, respectively. 14.07%, 27.01%, and 29.26% of the region were found to have very low, low, and moderate zones in danger of flooding. The

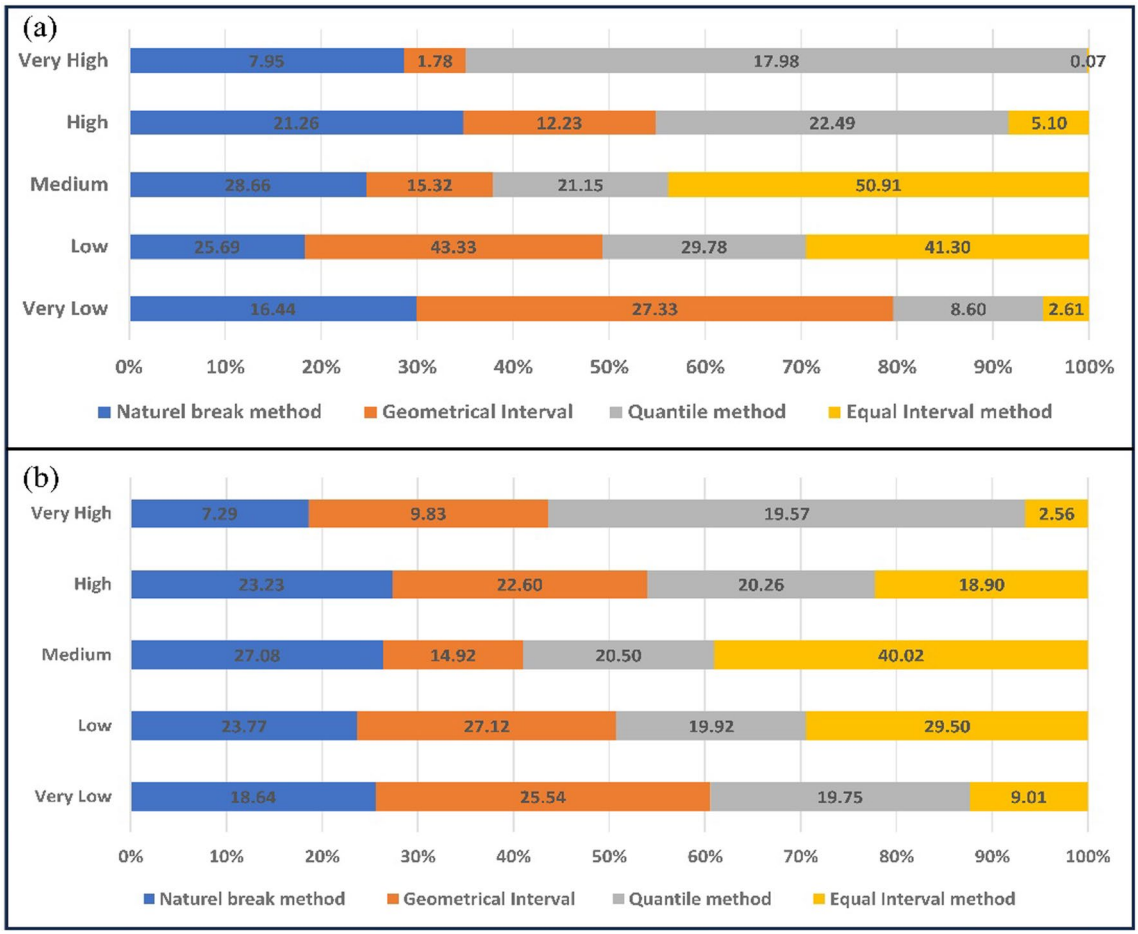

Fig. 7 **a** Classification of FSZ, **b** classification of FVZ

very high and high-risk areas are El-Dakahlyia and Damietta. Most of El-Qalubia lies in low risk.

The equal interval, quantile, geometrical interval, and natural break methods revealed the percentage-wise distribution of susceptibility classes and vulnerability classes, as shown in Fig. 7. For the FSZ, the geometrical interval approach produced the very low class, and the equal interval method produced the greatest medium and low classes. In contrast, the quantile deviation methodology produced the maximal coverage area of the very high and high flood susceptibility classes. In the FVZ, the quantile deviation methodology revealed the highest levels of flood risk for the very high and high classes. At the same time, the geometrical interval method represented the very low class, and the equal interval method represented the medium and low classes.

Table 9 Statistics of SPSA of FSP

Parameters	Empirical weight (%)	Effective weight (%)			
		Min	Max	Mean	SD
Elevation	26.7	5.23	68.41	37.27	7.92
Slope	19.2	4.03	71.89	28.75	5.69
TPI	1.5	0.14	7.57	1.21	0.88
TWI	8.7	0.99	26.74	4.50	1.50
NDVI	2.8	0.40	9.53	1.83	1.14
MNDWI	6.3	0.78	16.95	2.92	1.55
DD	12.3	1.49	39.64	8.33	5.39
DR	12.2	1.12	41.54	6.02	5.64
STI	1.5	0.11	8.69	2.54	0.94
SPI	1.5	0.11	8.69	2.52	0.95
MFI	4.4	0.53	17.82	3.49	2.27
Lithology	2.8	0.21	13.53	0.62	0.89

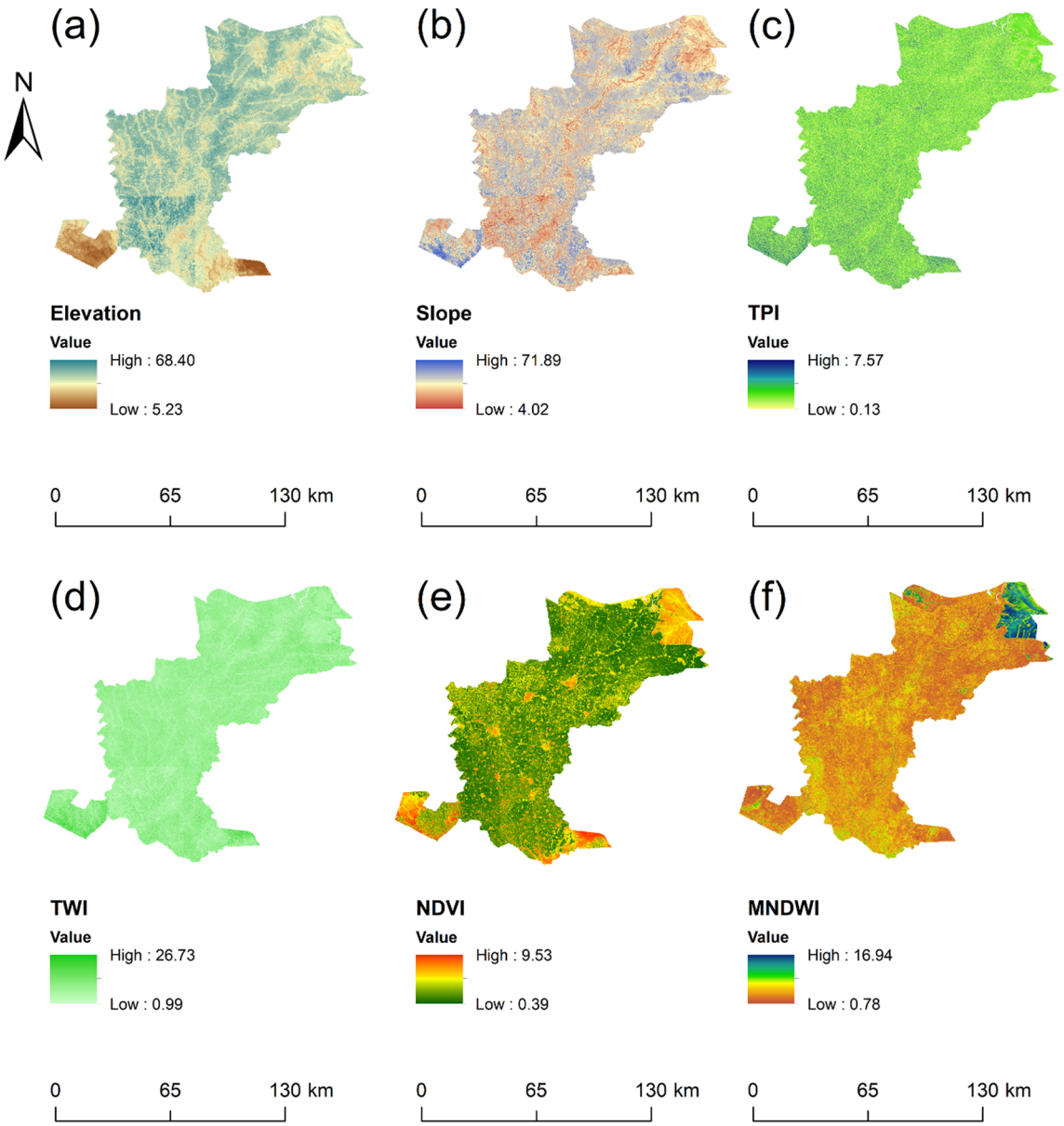

Fig. 8 The effective weight (W) of six FSPs utilized in this research: **a** elevation, **b** slope, **c** TWI, **d** TPI, **e** NDVI, and **f** MNDWI

Sensitivity analysis of the AHP method

To validate the AHP-provided weights using the APH approach, the implementation of sensitivity analysis is necessary [43, 47].

SPSA

Table 9 presents the result of the SPSA method for FSP. According to our findings, there are some differences between the W and the EW. The effective weights used in the SPSA (Table 9) reveal that elevation and slope were underestimated in the FSZ. Conversely, TPI, TWI, NDVI, MNDWI, DD, and DR were overestimated in the FSZ. Additionally, the results of effective weight estimation for SPI, STI, and MFI show a little discrepancy in the W values compared to the EW values, as can be seen from Table 9**.** Figures 8 and 9 illustrate the W map of twelve FSPs. SPSA revealed that elevation and slope layers were the most significant factors in the determination of FSP.

Table 10 demonstrates the result of the SPSA method for FVP. Our results show some differences in the W compared to the EW. The W used in the SPSA (Table 10) reveals that the total population and LULC were overestimated in the FVZ. Conversely, PD, DH, RD, and DTR were underestimated in the FVZ. Figure 10 shows

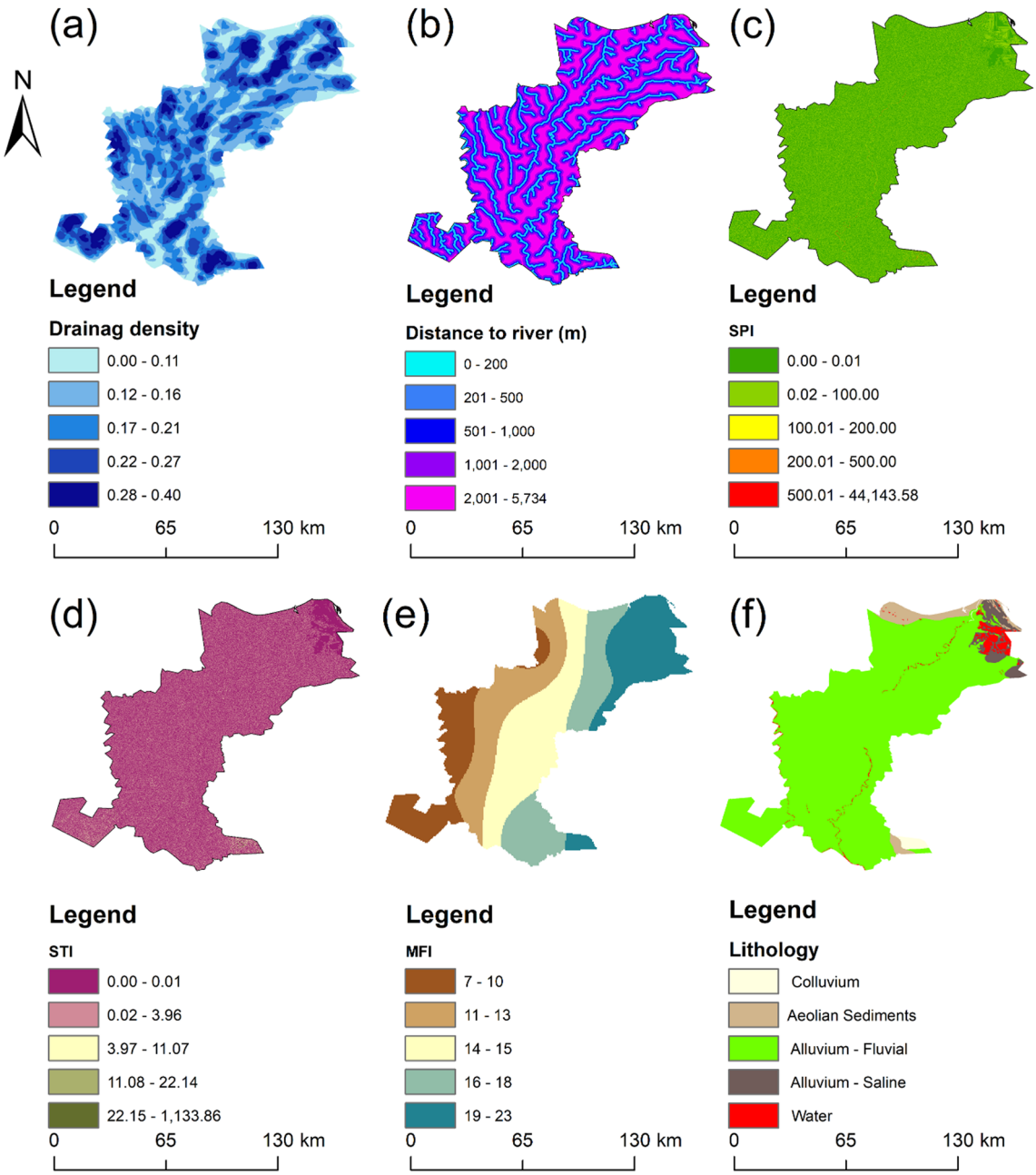

Fig. 9 The effective weight (W) of another six FSPs used in this research: **a** DD, **b** DR, **c** SPI, **d** STI, **e** MFI, and **f** lithology

the W map of the six FVPs. SPSA revealed that PD and TP thematical layers were the most significant factors in the flood vulnerability determination. As can be seen from Table 10, the road density was the lowest weight of the six FVPs.

MRSA

The MRSA results for FSP estimated by removing one parameter at a time are listed in Table 11**.** The higher variation index values were found after removing the Distance from the river layer, followed by TWI and lithology. The highest mean SI variation value (1.259%) is found when removing distance from the river. However, the lowest mean SI variation value (0.634%) is noticed when removing the slope. Figs. SM1 and SM2 in the SM describe the sensitivity index of the twelve FSPs used in this study. The proportion of FSZ maps that were created significantly varied as a result of removing

Table 10 Statistics of SPSA of FVP

Parameters	Empirical weight (%)	Effective weight (%)			
		Min	Max	Mean	SD
Total population	29.2	4.255	66.199	19.267	7.968
Population density (persons/km^2)	29.2	4.533	75.029	32.399	13.252
LULC	17.6	1.619	68.680	14.638	9.309
Distance to hospital (m)	10.7	1.250	49.611	15.622	9.409
Road density	5.9	0.934	31.862	7.690	4.018
Distance to road (m)	7.5	0.967	40.357	10.260	7.295

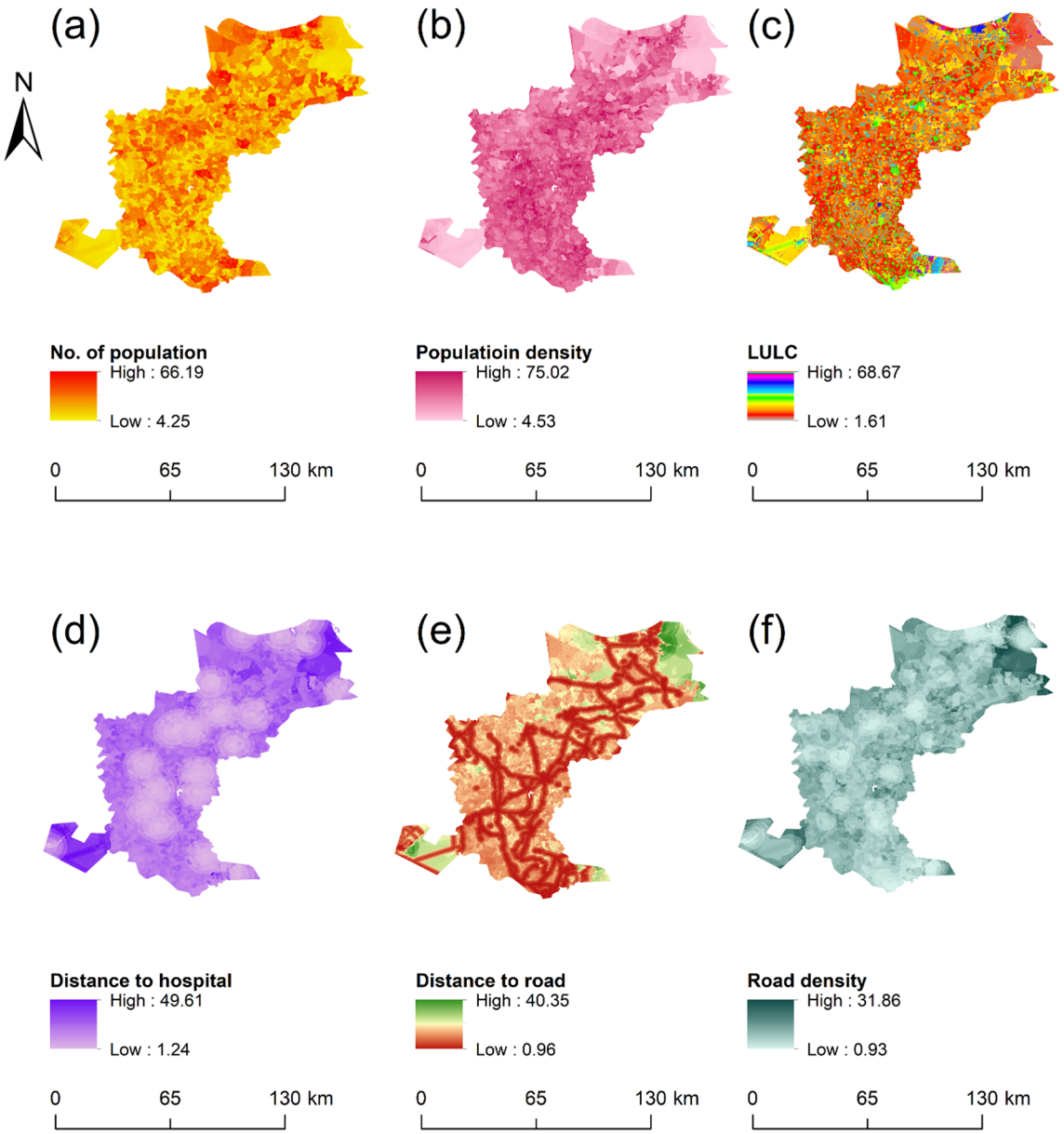

Fig. 10 The effective weight (W) of six FVPs used in this study: **a** TP, **b** PD, **c** LULC, **d** DH, **e** DTR, and **f** RD.

Table 11 Statistics of MRSA of FSP

Parameter removed	SI variation (%)			
	Min	Max	Mean	SD
Elevation	2.49E−06	4.283	0.822	0.635
Slope	3.93E−06	5.177	0.634	0.442
TPI	3.76E−01	1.401	1.036	0.115
TWI	3.38E−05	1.646	1.243	0.158
NDVI	1.32E−01	1.433	1.065	0.127
MNDWI	7.40E−04	1.537	1.109	0.152
DD	2.58E−06	2.094	1.091	0.442
DR	5.52E−07	2.356	1.259	0.429
STI	3.36E−01	1.295	0.875	0.091
SPI	2.89E−01	1.199	0.877	0.091
MFI	6.59E−07	1.917	1.001	0.232
Lithology	1.21E−04	1.566	1.183	0.112

each theme layer, as highlighted in Fig. SM3 in the SM and Table 12. Table 12 indicates the percentage of FSZ changes as each parameter is removed. MRSA further showed that the removal of the elevation and slope layers increases the very low FSZ area by 42.95% and 24.73% and the low FSZ area by 17.32% and 7.18%, respectively, as tabulated in Table 12. The largest increases of the very low, low, medium, high, and very high flood-prone areas are detected in the removal of elevation (42.95%), elevation (17.32%), slope (10.42%), distance from the river (11.02%), and NDVI (6.41%), respectively. The very low, medium, high, and very high flood-prone areas also decrease the most in exclusion of the MFI (− 3.37%),

Table 12 The percentage of FSZ changes as each parameter is removed

Parameters removed	FSZ (%)				
	Very low	Low	Medium	High	Very high
Elevation	42.95	17.32	0.45	− 38.30	− 44.02
Slope	24.73	7.18	10.42	− 32.98	− 23.23
TPI	2.44	1.15	0.94	− 4.41	− 0.37
TWI	0.16	0.97	5.18	− 7.74	− 1.45
NDVI	2.39	0.48	− 3.27	− 0.42	6.41
MNDWI	− 2.74	0.75	− 3.32	3.46	5.97
DD	20.88	4.51	− 6.90	− 7.10	− 13.87
DR	12.41	3.04	− 15.21	11.02	− 10.13
STI	4.23	4.16	1.90	− 9.13	− 4.59
SPI	4.34	4.08	1.63	− 9.45	− 2.73
MFI	− 3.37	0.78	2.59	0.55	2.02
Lithology	− 1.48	1.54	− 2.16	0.51	5.90

'+' indicates increased by area and '−' indicates decreased by area

Table 13 Statistics of MRSA of FVP

Parameters removed	SI variation (%)			
	Min	Max	Mean	SD
Total population	− 35.4033	7.1047	− 6.1259	2.3925
Population density	− 10.5007	9.7207	− 2.3050	3.6852
Distance to hospital	− 22.9092	5.4086	2.8678	2.2893
LULC	− 27.2932	8.9878	− 4.5407	2.5453
Road density	− 20.9755	6.2315	− 2.9369	1.3728
Distance to road	− 79.7511	12.4246	− 2.8645	2.0838

Distance from the river (− 15.21%), elevation (− 38.30%), and elevation (− 44.02%), respectively.

The MRSA results for FVP estimated by removing one parameter at a time are listed in Table 13. The higher variation index values were found after removing the Distance to the hospital. The highest mean SI variation value (2.87%) is found when removing the distance to the hospital. However, the lowest mean SI variation value (− 6.13%) is noticed when removing the total population despite the considerable "theoretical" weight attached to it. Fig. SM4 in the SM describes the sensitivity index of the six FVPs used in this study. Fig. SM5 in the SM shows the FVZ with the removal of each parameter.

Table 14 indicates the percentage of FSZ changes as each parameter is removed. MRSA further revealed that the removal of the LULC layer decreases the very low FSZ area by 43.52% and increases the very high FSZ area by 70.60%, as tabulated in Table 14. When population density (24.72%), total population (11.66%), LULC (57.09%), and total population (70.60%) are removed, the greatest increases are found in the low, medium, high, and very high flood-prone areas. The very low, low, medium, and high flood-prone areas also decrease the most in exclusion of the LULC (− 43.52%), LULC

Table 14 The percentage of FVZ changes as each parameter is removed

Parameters removed	FVZ (%)				
	Very low	Low	Medium	High	Very high
Total population	− 40.00	0.94	11.66	− 8.56	70.60
Population density	− 3.47	24.72	− 4.62	− 20.05	8.40
Distance to hospital	− 19.84	− 3.69	3.24	2.72	42.06
LULC	− 43.52	− 30.42	8.41	57.09	7.68
Road density	− 19.84	− 3.69	3.24	2.72	42.06
Distance to road	− 14.08	− 8.09	6.60	11.15	2.26

'+' indicates increased by area and '−' indicates decreased by area

Table 15 Comparison of weights for FSZ using various methods

Parameters	Saaty 1980		Stillwell 1981			
	Pairwise		Rank sum (RS)		Rank reciprocal (RR)	
	Direct rank	AHP	$n - R_j + 1$	$W_i(RS)$	$\frac{1}{R_j}$	$W_i(RR)$
Elevation	1	0.267	12	0.20	1	0.25
Slope	2	0.192	11	0.18	0.5	0.12
TWI	5	0.087	8	0.13	0.20	0.05
TPI	9	0.015	4	0.07	0.11	0.03
NDVI	8	0.028	5	0.08	0.13	0.03
MNDWI	6	0.063	7	0.11	0.17	0.04
Drainage density	3	0.123	10	0.16	0.33	0.08
Distance from river	4	0.122	9	0.15	0.25	0.06
SPI	9	0.015	4	0.07	0.11	0.03
STI	9	0.015	4	0.07	0.11	0.03
MFI	7	0.044	6	0.10	0.14	0.04
Lithology	8	0.028	5	0.08	0.13	0.03

Table 16 Comparison of weights for FVZ using various methods

Parameters	Saaty 1980		Stillwell 1981			
	Pairwise		Rank sum (RS)		Rank reciprocal (RR)	
	Direct rank	AHP	$n - R_j + 1$	$W_i(RS)$	$\frac{1}{R_j}$	$W_i(RR)$
Total population	1	0.292	5	0.08	1	0.25
Population density	1	0.292	5	0.08	1	0.25
LULC	2	0.176	4	0.07	0.50	0.12
Distance to hospital	3	0.107	3	0.05	0.33	0.08
Distance to road	4	0.075	2	0.03	0.25	0.06
Road density	5	0.059	1	0.02	0.20	0.05

(− 30.42%), population density (− 4.62%), and population density (− 20.05%), respectively.

Stillwell ranking methods

Tables 15 and 16 present a side-by-side comparison of the weightage assigned to criteria for FSZ using two different methods: Saaty's method from 1980 and Stillwell's method from 1981. The focus here is on assessing any variations in the criteria ranking and the resulting weights when applying these two distinct techniques. Upon examination of the tables, it is noted that no notable variations exist in the ranking of criteria between Saaty's method and Stillwell's method. In other words, the order of importance or preference assigned to the criteria remains relatively consistent across both methods.

However, it is noted that the weights associated with each criterion may undergo some modifications when utilizing Stillwell's techniques. The adjustments in weights are determined by applying the rank sum weight (Eq. 21) and reciprocal rank weight (Eq. 22) formulas as outlined in Stillwell's methodology. Despite these modifications, the overall ranking of criteria in terms of importance appears to be largely unchanged. In essence, the analysis suggests that while Stillwell's method may introduce some adjustments to the weights of criteria, the fundamental order of importance among the criteria for FSZ and FVZ remains similar when compared to Saaty's method. This information provides insights into the consistency or stability of the criteria ranking across different evaluation methodologies.

Validation of the model

Using the flood inventory map and ROC-AUC, the study statistically verified the AHP result. The 'ArcSDM' tool inside the ArcGIS platform was utilized to compare the map of FSZ with flooded points and non-flooded locations in order to determine the ROC-AUC. Figure 11 introduces the ROC curve and speedometer, showing the AUC for the AHP result. An AUC can evaluate

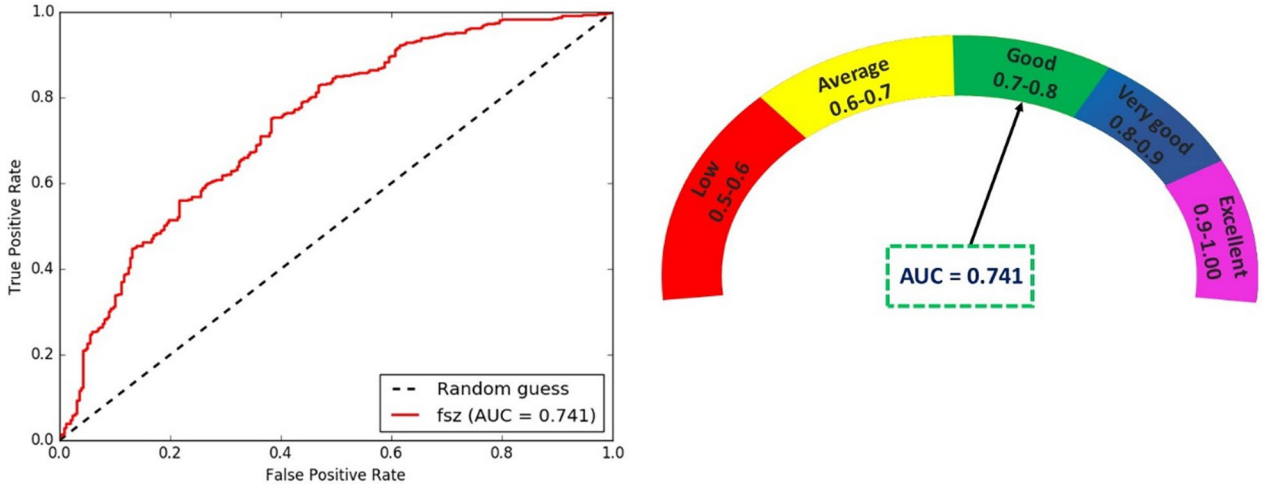

Fig. 11 ROC curve and speedometer showing the AUC

the accuracy of the prediction model's outcomes. The accuracy of the model increases with increasing AUC values and vice versa. An AUC value equal to or less than 0.5 denotes that the model is unsuitable for the study, while an AUC value near 1 denotes the ideal model with the maximum accuracy. This study found that the AHP technique's observed accuracy is 0.741 (74.10%). As a result, the model effectively generates the FRZ map, and it is regarded as a successful conclusion.

Discussion

Flooding is a major global problem due to its potential to cause substantial losses to people's livelihoods, houses, and economies. The present study effectively delineated FSZ, FVZ, and FRZ in Nile districts of the Damietta branch of Egypt using an integrated RS and GIS approach-based AHP technique. Also successfully determined the most effective parameters using single parameter sensitivity analysis, map removal sensitivity analysis and Stillwell ranking techniques.

The AHP method, known for its reliable effectiveness, was utilized to calculate pairwise comparisons and determine the priority of flood danger characteristics based on the weighted coefficients. Expert judgment has been used in several research to establish the conditioning parameters' weighting. Elevation, slope, TWI, drainage density, and distance to the river were identified as the most effective parameters for mapping flood susceptibility. In contrast, the distribution of the people, population density, LULC, and distance to the hospital were the most significant vulnerability factors, consistent with the finding of Mitra et al. [8]. Osman and Das also identified elevation, slope, drainage density, and river proximity as important factors in preparing flood prediction map [52]. Bui et al. emphasized that the areas close to the river are more susceptible to flooding, and it has been demonstrated that increasing the distance from the river can significantly lower the flood risks [1]. The agreement between these studies and our findings showed the robustness our methodology.

However, the causes of the most disagreement and uncertainty are often the criteria ratings or weights. Therefore, sensitivity analysis is essential to validate the weights assigned for AHP [43, 47]. Our study used three different sensitivity analyses, confirming the results of AHP such as Stillwell ranking techniques, single parameter sensitivity analysis and map removal sensitivity analysis. The single parameter sensitivity analysis shows the deviation between the empirical and effective weights, whereas map removal sensitivity analysis illustrates the sensitivity index among all parameters. This result confirms the results of Mitra et al. (2022), which evaluated the APH with sensitivity analysis [16].

Five primary flood risk groups were prepared, such as very high, high, moderate, low, and very low risk zones using natural breaking technique. Compared to the widely used natural breaks, where some classes may have a limited or excessive number of values, the quantile classification approach, which divides the values into groups that include an equal number of values, is preferable [53]. The model's accuracy would probably rise with more factors, but this also depends on the research region and the availability of the datasets containing the

input conditioning factors. Furthermore, in addition to the availability and choice of conditioning factor datasets, the output of susceptibility maps may also be influenced by the better resolution of the input datasets [53].

Although flooding cannot be completely avoided, it may be minimized by adopting the appropriate safety measures. This objective necessitates accurate diagnosis of susceptible, vulnerable, and risky regions, which is the main concern for design reasons. The basis for additional analysis, such as risk and hazard mapping, is provided by flood susceptibility maps [54]. Disaster management and planning authorities may utilize the study to determine which regions are most likely to flood and to take the appropriate preventative and corrective action to lessen the damage that floods cause. Flood-prone locations can be identified, and the necessary structural and non-structural solutions can be implemented to mitigate losses associated with floods by mapping FRZ [55].

However, the current approach's limitations include the lack of temporal variations and real-time flood data. One of the primary limitations of the current study was that, although some other studies, like Tehrany et al. [56] and Khosravi et al. [55] had done the same, the identification of non-flooding locations was done using Google Earth rather than a field survey. The study's limitations are implied by the MCDA approach, which may be further adjusted by utilizing high-resolution data and other methods that are appropriate for this area. The high resolution of LIDAR DEM would have also had a major influence on the models' performance and predictive capability, thus more study should be conducted using that data rather than ASTER DEM. By using machine learning approaches, the research may also make better judgments by having a greater understanding of the locations that are risk-prone, susceptible to flooding, and vulnerable. In order to improve flood prediction, future research recommendations include a thorough comparative analysis that evaluates the simplicity and accuracy of various machine learning, data mining, multivariate, bivariate, and multicriteria decision-making models and their ensembles. As with every research, there is a chance of inaccuracy and uncertainty in the current study's findings because of factors such as flood-influencing factors. Further study is necessary for each of these factors to show how these uncertainties affect the final flood susceptibility maps. Future studies should take these uncertainties into account by selecting additional flood factors, including daily or sub-daily rainfall, and categorizing the flood factors in cooperation with stakeholder [57]. Additional sensitivity analyses might be included in the study to enhance the model evaluation.

Conclusions

This study utilized the AHP technique and sensitivity analysis for delineating flood risk zonation in Nile districts of the Damietta branch of Egypt based on flood susceptibility and flood vulnerability. Furthermore, 12 susceptibility parameters are used for producing FSZ, and six vulnerability parameters are used for producing FVZ. Using GIS software, the final flood risk map is produced by combining vulnerability and hazard zonation.

The findings indicate no multicollinearity problem between the various susceptibility and vulnerability parameters. In this study, elevation (27%), slope (19%), drainage density (12%), distance to the river (12%), and TWI (09%) were the most prominent factors in estimating the FSZ. Furthermore, the FVZ was primarily determined by three factors: total population (29%), population density (29%), and LULC (18%). In this study, the AUC is used to assess the effectiveness and performance of the AHP approach with a 74.1% accuracy rate.

According to the results, the area covered by the high and very high flood risk classes was 21.40 and 8.26%, respectively. Within the research region, the very low, low, and moderate flood risk zones were found at 14.07, 27.01, and 29.26%. The very high and high-risk areas are El-Dakahlyia and Damietta. Most of El-Qalubia lies in low risk. Thus, in order to enhance the area, a sufficient flood risk plan is needed. Additionally, it is advised that high-risk areas adjust their flood defense strategies. When comparing Stillwell's technique to Saaty's method, the study indicates that although certain modifications to the criterion weights may be produced, the fundamental order of significance between the FSZ and FVZ criteria does not change.

Lastly, this study offers promising results about our understanding of mapping and assessing flood risk zones. However, there are a few limitations that should be mentioned. Experts' weight assignments to the factors in the MCDA may lead to bias in the final maps. Moreover, the majority of the variables were taken from medium-resolution remote sensing data, which may have reduced the accuracy of the flood prediction.

Using high-resolution data and other appropriate techniques, the MCDA technique may be further refined to address the limits of the research. Additional sensitivity analyses might be incorporated into the study to enhance the model evaluation. In addition, using parameters derived from LiDAR by employing advanced machine learning techniques is recommended to enhance understanding of flood susceptibility, vulnerability, and risk-prone areas, the study might potentially lead to more informed conclusions. For future studies, this research must be coupled with

hydraulic modeling to provide 2D maps for both depth and velocity. Decision-makers can thus use this map as a guide for possible preventative actions, improved land use planning, and flood risk management in the context of climate change. To effectively execute risk-reduction methods, land-use planners and government authorities might benefit from having an accurate FSZ, FVZ, and FRZ.

Supplementary Information

The online version contains supplementary material available at https://doi.org/10.1186/s12302-024-01001-9.

Supplementary Material 1.

Author contributions

Mohamed Zhran: writing—review and editing, writing—original draft, visualization, validation, software, methodology, investigation, formal analysis, data curation, conceptualization. Karim Ghanem: visualization, validation, software, formal analysis. Aqil Tariq: writing—review and editing. Fahad Alshehri: writing—review and editing. Shuanggen Jin:: investigation, writing—review and editing. Jayanta Das: validation, writing—review and editing. Chaitanya Baliram Pande: writing—review and editing. Malay Pramanik: writing—review and editing. Fahdah Falah Ben Hasher: writing—review and editing. Ashraf Mousa: writing—review and editing.

Funding

Open access funding provided by The Science, Technology & Innovation Funding Authority (STDF) in cooperation with The Egyptian Knowledge Bank (EKB). Not applicable.

Data availability

All data generated or analyzed during this study are included in this published article.

Declarations

Competing interests

The authors declare no competing interests.

Received: 11 May 2024 Accepted: 22 September 2024
Published online: 15 October 2024

References

1. Bui DT, Khosravi K, Shahabi H et al (2019) Flood spatial modeling in Northern Iran using remote sensing and GIS: a comparison between evidential belief functions and its ensemble with a multivariate logistic regression model. Remote Sens (Basel). https://doi.org/10.3390/rs11131589
2. Parsian S, Amani M, Moghimi A et al (2021) Flood hazard mapping using fuzzy logic, analytical hierarchy process, and multi-source geospatial datasets. Remote Sens (Basel). https://doi.org/10.3390/rs13234761
3. Rahmati O, Zeinivand H, Besharat M (2016) Flood hazard zoning in Yasooj region, Iran, using GIS and multi-criteria decision analysis. Geomat Nat Haz Risk 7:1000–1017. https://doi.org/10.1080/19475705.2015.1045043
4. Taylor J, Lai K man, Davies M, et al (2011) Flood management: prediction of microbial contamination in large-scale floods in urban environments. Environ Int 37:1019–1029
5. Veerbeek W, Zevenbergen C (2009) Deconstructing urban flood damages: Increasing the expressiveness of flood damage models combining a high level of detail with a broad attribute set. J Flood Risk Manag 2:45–57. https://doi.org/10.1111/j.1753-318X.2009.01021.x
6. Merz B, Kreibich H, Schwarze R, Thieken A (2010) Review article "assessment of economic flood damage." Nat Hazards Earth Syst Sci 10:1697–1724
7. Souissi D, Zouhri L, Hammami S et al (2020) GIS-based MCDM–AHP modeling for flood susceptibility mapping of arid areas, southeastern Tunisia. Geocarto Int 35:991–1017. https://doi.org/10.1080/10106049.2019.1566405
8. Mitra R, Saha P, Das J (2022) Assessment of the performance of GIS-based analytical hierarchical process (AHP) approach for flood modelling in Uttar Dinajpur district of West Bengal, India. Geomat Nat Haz Risk 13:2183–2226. https://doi.org/10.1080/19475705.2022.2112094
9. Hammami S, Zouhri L, Souissi D et al (2019) Application of the GIS based multi-criteria decision analysis and analytical hierarchy process (AHP) in the flood susceptibility mapping (Tunisia). Arab J Geosci. https://doi.org/10.1007/s12517-019-4754-9
10. Waqas H, Lu L, Tariq A et al (2021) Flash flood susceptibility assessment and zonation using an integrating analytic hierarchy process and frequency ratio model for the Chitral district, Khyber Pakhtunkhwa, Pakistan. Water (Switzerland). https://doi.org/10.3390/w13121650
11. Sarkar D, Mondal P (2020) Flood vulnerability mapping using frequency ratio (FR) model: a case study on Kulik river basin, Indo-Bangladesh Barind region. Appl Water Sci. https://doi.org/10.1007/s13201-019-1102-x
12. Samanta S, Pal DK, Palsamanta B (2018) Flood susceptibility analysis through remote sensing, GIS and frequency ratio model. Appl Water Sci. https://doi.org/10.1007/s13201-018-0710-1
13. AlAli AM, Salih A, Hassaballa A (2023) Geospatial-based analytical hierarchy process (AHP) and weighted product model (WPM) techniques for mapping and assessing flood susceptibility in the Wadi Hanifah Drainage Basin, Riyadh Region. Saudi Arabia Water (Switzerland). https://doi.org/10.3390/w15101943
14. Hoque MAA, Tasfia S, Ahmed N, Pradhan B (2019) Assessing spatial flood vulnerability at Kalapara upazila in Bangladesh using an analytic hierarchy process. Sensors (Switzerland). https://doi.org/10.3390/s19061302
15. Zou Q, Zhou J, Zhou C et al (2013) Comprehensive flood risk assessment based on set pair analysis-variable fuzzy sets model and fuzzy AHP. Stoch Env Res Risk Assess 27:525–546. https://doi.org/10.1007/s00477-012-0598-5
16. Mitra R, Das J (2023) A comparative assessment of flood susceptibility modelling of GIS-based TOPSIS, VIKOR, and EDAS techniques in the Sub-Himalayan foothills region of Eastern India. Environ Sci Pollut Res 30:16036–16067. https://doi.org/10.1007/s11356-022-23168-5
17. Al-Aizari AR, Al-Masnay YA, Aydda A et al (2022) Assessment analysis of flood susceptibility in tropical desert area: a case study of Yemen. Remote Sens (Basel). https://doi.org/10.3390/rs14164050
18. Saaty RW (1987) The analytic hierarchy process-what it is and how it is used
19. Rincón D, Khan UT, Armenakis C (2018) Flood risk mapping using GIS and multi-criteria analysis: A greater Toronto area case study. Geosciences (Switzerland). https://doi.org/10.3390/geosciences8080275
20. Birkmann J (2007) Risk and vulnerability indicators at different scales: Applicability, usefulness and policy implications. Environ Hazards 7:20–31. https://doi.org/10.1016/j.envhaz.2007.04.002
21. Monte BEO, Goldenfum JA, Michel GP, de Cavalcanti JRA (2021) Terminology of natural hazards and disasters: a review and the case of Brazil. Int J Disaster Risk Reduct. https://doi.org/10.1016/j.ijdrr.2020.101970
22. Feldmeyer D, Birkmann J, McMillan JM et al (2021) Global vulnerability hotspots: differences and agreement between international indicator-based assessments. Clim Change. https://doi.org/10.1007/s10584-021-03203-z
23. Gebremichael E, Sultan M, Becker R et al (2018) Assessing land deformation and sea encroachment in the Nile delta: a radar interferometric and inundation modeling approach. J Geophys Res Solid Earth 123:3208–3224. https://doi.org/10.1002/2017JB015084
24. The International Federation of Red Cross and Red Crescent Societies (2020) Emergency Plan of Action (EPoA) Egypt: Flash Floods
25. (2023) https://weatherandclimate.com/. In: Weather and Climate
26. Tehrany MS, Jones S, Shabani F (2019) Identifying the essential flood conditioning factors for flood prone area mapping using machine learning techniques. Catena (Amst) 175:174–192. https://doi.org/10.1016/j.catena.2018.12.011

27. Fernández DS, Lutz MA (2010) Urban flood hazard zoning in Tucumán Province, Argentina, using GIS and multicriteria decision analysis. Eng Geol 111:90–98. https://doi.org/10.1016/j.enggeo.2009.12.006
28. Aldileemi H, Zhran M, El-Mewafi M (2023) Geospatial monitoring and prediction of land use/land cover (LULC) dynamics based on the CA-Markov simulation model in Ajdabiya, Libya. IJG 19:15–29. https://doi.org/10.52939/ijg.v19i12.2973
29. Chen Y, Wang D, Zhang L et al (2023) Flood risk assessment of Wuhan, China, using a multi-criteria analysis model with the improved AHP-Entropy method. Environ Sci Pollut Res 30:96001–96018. https://doi.org/10.1007/s11356-023-29066-8
30. Shahabi H, Shirzadi A, Ronoud S et al (2021) Flash flood susceptibility mapping using a novel deep learning model based on deep belief network, back propagation and genetic algorithm. Geosci Front. https://doi.org/10.1016/j.gsf.2020.10.007
31. Beven KJ, Kirkby MJ (1979) A physically based, variable contributing area model of basin hydrology. Hydrol Sci Bull 24:43–69. https://doi.org/10.1080/02626667909491834
32. Rahmati O, Kalantari Z, Samadi M et al (2019) GIS-based site selection for check dams in watersheds: Considering geomorphometric and topo-hydrological factors. Sustainability (Switzerland). https://doi.org/10.3390/su11205639
33. Powell SJ, Jakeman A, Croke B (2014) Can NDVI response indicate the effective flood extent in macrophyte dominated floodplain wetlands? Ecol Indic 45:486–493. https://doi.org/10.1016/j.ecolind.2014.05.009
34. Xu H (2006) Modification of normalised difference water index (NDWI) to enhance open water features in remotely sensed imagery. Int J Remote Sens 27:3025–3033. https://doi.org/10.1080/01431160600589179
35. Chapi K, Singh VP, Shirzadi A et al (2017) A novel hybrid artificial intelligence approach for flood susceptibility assessment. Environ Model Softw 95:229–245. https://doi.org/10.1016/j.envsoft.2017.06.012
36. Butler D, Kokkalidou A, Makropoulos Ck (2006) Supporting the siting of new urban developments for integrated urban water resource management. In: Integrated Urban Water Resources Management. Kluwer Academic Publishers, pp 19–34
37. Vafakhah M, Mohammad Hasani Loor S, Pourghasemi H, Katebikord A (2020) Comparing performance of random forest and adaptive neuro-fuzzy inference system data mining models for flood susceptibility mapping. Arab J Geosci. https://doi.org/10.1007/s12517-020-05363-1
38. Grayson RB, Ladson DAR (1991) Digital terrain modelling: a review of hydrological, geomorphological, and biological applications
39. Ali SA, Parvin F, Pham QB et al (2020) GIS-based comparative assessment of flood susceptibility mapping using hybrid multi-criteria decision-making approach, naïve Bayes tree, bivariate statistics and logistic regression: a case of Topľa basin, Slovakia. Ecol Indic. https://doi.org/10.1016/j.ecolind.2020.106620
40. Costache R (2019) Flash-flood Potential Index mapping using weights of evidence, decision Trees models and their novel hybrid integration. Stoch Env Res Risk Assess 33:1375–1402. https://doi.org/10.1007/s00477-019-01689-9
41. Srivastava PK, Han D, Rico-Ramirez MA, Islam T (2014) Sensitivity and uncertainty analysis of mesoscale model downscaled hydro-meteorological variables for discharge prediction. Hydrol Process 28:4419–4432. https://doi.org/10.1002/hyp.9946
42. Costache R, Popa MC, Tien Bui D et al (2020) Spatial predicting of flood potential areas using novel hybridizations of fuzzy decision-making, bivariate statistics, and machine learning. J Hydrol (Amst). https://doi.org/10.1016/j.jhydrol.2020.124808
43. Mukherjee I, Singh UK (2020) Delineation of groundwater potential zones in a drought-prone semi-arid region of east India using GIS and analytical hierarchical process techniques. Catena (Amst). https://doi.org/10.1016/j.catena.2020.104681
44. Saha S (2017) Groundwater potential mapping using analytical hierarchical process: a study on Md. Bazar Block of Birbhum District, West Bengal. Spat Inf Res 25:615–626. https://doi.org/10.1007/s41324-017-0127-1
45. Saaty TL, Katz JM (1990) How to make a decision: The Analytic Hierarchy Process
46. Zghibi A, Merzougui A, Chenini I et al (2016) Groundwater vulnerability analysis of Tunisian coastal aquifer: an application of DRASTIC index method in GIS environment. Groundw Sustain Dev 2–3:169–181. https://doi.org/10.1016/j.gsd.2016.10.001
47. Fenta AA, Kifle A, Gebreyohannes T, Hailu G (2015) Spatial analysis of groundwater potential using remote sensing and GIS-based multi-criteria evaluation in Raya Valley, northern Ethiopia. Hydrogeol J 23:195–206. https://doi.org/10.1007/s10040-014-1198-x
48. Kindie AT, Enku T, Moges MA, et al (2019) Spatial analysis of groundwater potential using gis based multi criteria decision analysis method in Lake Tana Basin, Ethiopia. In: Lecture Notes of the Institute for Computer Sciences, Social-Informatics and Telecommunications Engineering, LNICST. Springer Verlag, pp 439–456
49. Stillwell WG, Seaver DA (1981) A comparison of weight approximation techniques in multiattribute utility decision making
50. Arabameri A, Rezaei K, Cerdà A et al (2019) A comparison of statistical methods and multi-criteria decision making to map flood hazard susceptibility in Northern Iran. Sci Total Environ 660:443–458. https://doi.org/10.1016/j.scitotenv.2019.01.021
51. Saha S, Sarkar D, Mondal P (2022) Efficiency exploration of frequency ratio, entropy and weights of evidence-information value models in flood vulnerability assessment: a study of Raiganj subdivision, Eastern India. Stoch Env Res Risk Assess 36:1721–1742. https://doi.org/10.1007/s00477-021-02115-9
52. Osman SA, Das J (2023) GIS-based flood risk assessment using multi-criteria decision analysis of Shebelle River Basin in southern Somalia. SN Appl Sci. https://doi.org/10.1007/s42452-023-05360-5
53. Gudiyangada Nachappa T, Tavakkoli Piralilou S, Gholamnia K et al (2020) Flood susceptibility mapping with machine learning, multi-criteria decision analysis and ensemble using Dempster Shafer Theory. J Hydrol (Amst) 590:125275
54. Tehrany MS, Pradhan B, Mansor S, Ahmad N (2015) Flood susceptibility assessment using GIS-based support vector machine model with different kernel types. Catena (Amst) 125:91–101. https://doi.org/10.1016/j.catena.2014.10.017
55. Khosravi K, Shahabi H, Pham BT et al (2019) A comparative assessment of flood susceptibility modeling using Multi-Criteria Decision-Making Analysis and Machine Learning Methods. J Hydrol (Amst) 573:311–323. https://doi.org/10.1016/j.jhydrol.2019.03.073
56. Tehrany MS, Pradhan B, Jebur MN (2015) Flood susceptibility analysis and its verification using a novel ensemble support vector machine and frequency ratio method. Stoch Env Res Risk Assess 29:1149–1165. https://doi.org/10.1007/s00477-015-1021-9
57. Ahmadisharaf E, Kalyanapu AJ, Chung ES (2017) Sustainability-based flood hazard mapping of the Swannanoa River watershed. Sustainability (Switzerland). https://doi.org/10.3390/su9101735

Publisher's Note